Electronic resonance enhancement of coherent anti-Stokes Raman scattering

S. A. J. Druet, B. Attal, T. K. Gustafson,* and J. P. Taran
Office National d'Études et de Recherches Aérospatiales, 92320 Châtillon, France
(Received 7 November 1977; revised manuscript received 4 May 1978)

We analyze the enhancement of the coherent anti-Stokes Raman-scattering (CARS) susceptibility when the frequencies of the waves involved are tuned into resonance with discrete and continuum one-photon absorptions, and discuss the applications. We first derive the expression for the susceptibility by means of the usual iterative treatment of density-matrix perturbations. We then show that this derivation can be done in a straightforward manner by means of a time-ordered diagrammatic representation, which brings novel physical insight into CARS mechanisms. This representation can also be used to analyze the transient behavior of CARS as the pump fields are turned on and off. In addition, we discuss resonant CARS spectroscopy in the gas phase. The spectrum is composed of the expected enhanced Raman lines and also of double-electronic-resonance lines. All these lines occur as doublets. We derive their relative intensities based on detunings, collisional broadening, Franck-Condon overlap integrals, and rotational transition moments. The line contours are predicted by representing the susceptibility in the complex plane. The problems arising from saturation and the optical Stark effect are also considered; all should be small below pump densities of 100 MW/cm^2 in gas mixtures near STP. Fluorescence interference is negligible, except at power densities high enough for the Stark effect to be large. Beam absorption is also negligible at STP if the resonant species' concentration is less than 1000 ppm; phase matching is then satisfied. Finally, an experimental resonant CARS spectrum of I_2 at 1 mb in air near STP is presented and interpreted; the susceptibility is about 400 times larger than that of O_2 off resonance and under the same thermodynamic conditions.

I. INTRODUCTION

Coherent anti-Stokes Raman scattering (CARS) ranks among the most powerful optical tools for chemical analysis of gases in reactive media and for high-resolution molecular spectroscopy. CARS belongs to a family of related third-order optical mixing techniques such as the Raman induced Kerr effect[1-3] (RIKE) or stimulated Raman gain spectroscopy[4] (SRGS) which were proposed recently. All these techniques offer attractive alternatives to conventional Raman spectroscopy; their superiority over spontaneous Raman scattering (RS) comes from their coherent nature. In particular, the advantage of CARS is particularly striking when the spontaneous Raman emission is small compared to laser-induced fluorescence or chemiluminescence.[5-9] Thus, CARS has been used successfully in combustion diagnostics,[5,6] instantaneous turbulent combustion measurements[7] and in discharges in low-pressure gases.[8,9] It can also be used in plasmas studies for which RIKE was originally proposed. Using cw lasers, it has been applied to ultrahigh-resolution Raman spectroscopy in liquids[10] and gases,[11-14] a task for which SRGS also appears well suited. It has also permitted fluorescence-free resonant Raman spectra of biological samples to be obtained.[15,16] With picosecond lasers, it can be used as a diagnostics tool in fast relaxation processes,[17] reaction dynamics, spectroscopy of transient molecules in discharges[8,9] and excited-states studies.

CARS is characterized by a third-order nonlinear susceptibility $\chi^3(\omega_a)$. In general, the pump beams are focused, so that the anti-Stokes wave generation takes place near the focus; the anti-Stokes power P_a collected during a measurement is then independent of the focal length and reads, in the notation of[18]

$$P_a = [4\pi^2(\omega_a/c^2)]^2(\omega_L/\pi c)^2 P_L^2 P_S |\chi^{(3)}(\omega_a)|^2 , \qquad (1)$$

where P_L and P_S are the pump powers at ω_L and ω_S; $\chi^{(3)}(\omega_a)$ is the sum of a Raman resonant part χ_R contributed by the closest vibration-rotation resonances of the particular species which is being probed, and a slowly varying nonresonant contribution χ_{NR} from all the species. Delicate problems are posed in the interpretation of the spectra when $|\chi_R| \leq |\chi_{NR}|$. For that reason, the discrimination of a trace gas against the dominant species in a mixture is ultimately poorer in CARS than in RS. In practice, the detectivity limit is around 1000 ppm for most diatomic gases.[18,19] There are two ways of improving it. One is to reduce χ_{NR} with respect to χ_R by provoking destructive interferences between several contributions to χ_{NR}[10,20]; this, however, cannot be very useful in gases where rapid temperature and concentration fluctuations are often encountered. The other one, which is discussed in this paper, is to enhance χ_R with respect to χ_{NR} by tuning one or two of the three field frequencies to the electronic resonances of the molecules to be detected (resonant CARS).

The resonance condition can be achieved either near discrete absorption lines, or in the vibrational dissociative absorption continuum. The discussion will be generally restricted to the case of molecular species in the gas phase. The problems one encounters in the liquid phase are quite similar and, in many instances, less severe than in gases. Some characteristic differences, however, will be pointed out.

The calculation and physical interpretation of resonant susceptibility terms have been given great attention; particular attention has also been paid to the retrieval and interpretation of resonant CARS spectra; finally, preliminary experimental results have been analyzed. The work is divided as follows:

In Sec. II we derive a quantum-mechanical expression of $\chi^{(3)}(\omega_a)$ in order to display the influence of electronic resonance. For the case of resonances with discrete absorption lines, the calculation is carried out in the density-matrix formalism by means of the well known iterative treatment of time-dependent perturbations. The density-matrix formalism is convenient for the treatment of line-broadening mechanisms (Sec. II A).

It is shown in Sec. II B that the time-ordered diagrams of Yee and coworkers[21,22] are well suited for the treatment of resonant CARS. This representation brings new insight into the quantum-mechanical processes that create the anti-Stokes polarization. In particular, we address the problem of energy transfer between waves and molecules on resonance, as well as the spectral distortion resulting from some time-ordered terms previously included in χ_{NR}. Finally, we extend this analysis to the case of a resonance into a continuum (Sec. II C). This type of excitation presents interesting spectroscopic advantages which may prove useful for the study of rapidly fluctuating media.

In Sec. III we investigate the essential characteristics of resonant CARS spectra on the basis of the previous theory and discuss their application to analytical chemistry. We examine the spectral content for discrete and continuum resonances (Sec. III A). We show in Sec. III B that the line contour can be easily predicted by representing the susceptibility as a vector in the complex plane. Recent experimental results in liquids[16] are thus explained without resorting to numerical calculations. In Sec. III C, we consider in turn rotational selection rules, collisional broadening, population perturbations and the optical Stark effect, and discuss their influence upon CARS spectra. All these effects must be carefully considered when using resonant CARS in analytical chemistry. The detectivity improvement is also inferred through comparison with experimental results in resonant spontaneous Raman scattering (RRS).

In Sec. IV the diagrammatic representation is used to analyze the transient behavior of the CARS power as the pump fields are turned on and off. This behavior is of particular interest when short pulses are used. Significant differences from transients in RRS are predicted.

In Sec. V experimental results obtained in Iodine vapor are discussed in the light of the preceding models. Satisfactory agreement is found, notably with regards to spectral content and susceptibility enhancement.

II. QUANTUM-MECHANICAL DERIVATION OF $\chi^{(3)}(\omega_a)$ (STATIONARY CASE)

The creation of the anti-Stokes wave is due to a third-order coherent nonlinear polarization $\vec{P}_{NL}^{(3)}(\omega_a,t)$ induced in the medium at frequency $\omega_a = 2\omega_L - \omega_S$ by the pump beams. This polarization is strong whenever $\omega_L - \omega_S$ comes close to a Raman-active vibrational frequency ω_{ba}, and can be further enhanced if ω_L, ω_S, or ω_a comes close to some of the absorption frequencies of the molecules. This polarization is capable of generating a coherent wave at ω_a subject to growth and propagation as determined by Maxwell's equations; the latter problem will not be considered here, and we shall confine the discussion to the spectral and temporal properties of $\vec{P}_{NL}^{(3)}(\omega_a,t)$ and its associated susceptibility $\chi^{(3)}(\omega_a)$.

A. Density matrix

In order to account for the discrete electronic resonances; a calculation of $\vec{P}_{NL}^{(3)}(\omega_a,t)$ has been done using the density-matrix formalism; this calculation, which follows the approach used in Refs. 23 and 24, is only outlined here since similar treatments have been used in the past for the calculation of nonlinear susceptibilities (Refs. 25–29). The quantum state of the scattering molecules is represented, as is conventional, by the density operator $\rho(t)$ with the well-known equation of motion

$$\frac{\partial \rho(t)}{\partial t} = -\frac{i}{\hbar}[H_0 + V(t), \rho(t)] + \left.\frac{\partial \rho}{\partial t}\right|_{\text{damp}} . \qquad (2)$$

H_0 is the free molecule Hamiltonian with a discrete spectrum of eigenstates $|n\rangle$ corresponding to eigenenergies $\hbar\omega_n$; the Hamiltonian describing the interaction of the molecules with the radiation fields is $V(t) = -\vec{P}\cdot\vec{E}(t)$ in the dipolar approximation; $\vec{P}$ is the dipole moment operator and $\vec{E}(t)$ the instantaneous value of the electric field; $\partial\rho/\partial t|_{\text{damp}}$ is the damping term, which is determined by stochastic processes such as spontaneous emis-

sion of light and collisions between molecules. Several approximations are usually made on the collisional mechanisms, which leads to a simple expression for the damping terms.[24,30-32] These approximations are (i) the assumption of stationary stochastic processes, (ii) the impact approximation, and (iii) the isolated line approximation. Approximation (ii) is equivalent to assuming that the time interval between two collisions is larger than their duration. It is usually valid in gases; it allows one to replace the fluctuating time-dependent interactions between molecules by an effective time-independent interaction which is not Hermitian.[30] With approximation (iii) the coupling by relaxation among the off-diagonal matrix elements $\rho_{nn'}$ can be neglected. $\partial\rho/\partial t|_{\text{damp}}$ in (2) is then written[23,24]

$$\left.\frac{\partial\rho_{nn}}{\partial t}\right|_{\text{damp}} = -\Gamma_{nn}\rho_{nn} + \sum_{k\neq n} W_{nk}\rho_{kk} ,$$
$$\left.\frac{\partial\rho_{nn'}}{\partial t}\right|_{\text{damp}} = -\Gamma_{nn'}\rho_{nn'} , \tag{3}$$

with $\Gamma_{nn'} = \frac{1}{2}(\Gamma_{nn}+\Gamma_{n'n'}) + \Gamma^{e}_{nn'}$; Γ_{nn} is related to the finite lifetime π/Γ_{nn} of state $|n\rangle$ due to spontaneous emission and inelastic collisions, and $2\Gamma^{e}_{nn'}$ is the full broadening of the absorption line between states $|n\rangle$ and $|n'\rangle$ due to phase interrupting elastic collisions; W_{nk} is the transition probability via inelastic collisions between states $|k\rangle$ and $|n\rangle$. It is seen from (3) that the three approximations above [hereafter called approximation (3)] result in Lorentzian line broadening. Note also that approximation (iii) does not imply that the relaxation of states $|n\rangle$ (or $|n'\rangle$) to other states via inelastic collisions is negligible as can be seen in the first equation of (3); this approximation is valid if the condition $\Gamma_{nn'} < \omega_{nn'}$ is satisfied.[30]

Assuming that the perturbation $V(t)$ is weak enough to validate a solution of (2) expanded in successive powers of $V(t)$, the nonlinear polarization of interest $\vec{P}^{(3)}_{NL}(\omega_a, t)$ is, in a pure gas

$$\vec{P}^{(3)}_{NL}(\omega_a,t) = NT_r\rho^{(3)}(\omega_a,t)\vec{P} = N\sum_{m,n}\rho^{(3)}_{nm}(\omega_a,t)\vec{P}_{mn} , \tag{4}$$

where N is the number density of the molecules and $\rho^{(3)}_{nm}(\omega_a, t)$ is the third-order perturbation term of $\rho_{nm}(t)$ proportional to those terms of $[V(t)]^3$ at frequency ω_a. In the calculation, the radiation fields are taken in the form of quasimonochromatic plane waves traveling along the z axis, all with the same polarization so that the total field can be written

$$\vec{E}(z,t) = \hat{e}[E_L(z,t)\exp i(k_L z - \omega_L t) + E_S(z,t)\exp i(k_S z - \omega_S t) + E_a(z,t)\exp i(k_a z - \omega_a t)] + \text{c.c.} , \tag{5}$$

where k_L, k_S, and k_a are the usual propagation vectors at ω_L, ω_S, and ω_a, the field envelopes E_L, E_S, and E_a being slowly varying functions of z and t with $|E_a| \ll |E_L|, |E_S|$.

If the rise and fall times of the pump beams are long conpared to the $(\Gamma^{-1}_{nn'})$'s and (Γ^{-1}_{nn})'s, one does not need to take into account the transient solutions of Eq. (2) (the contribution of transients to the scattering can be important near resonance and will be studied in Sec. IV). The field envelopes $E_{L,S}(z,t)$ are thus assumed to be independent of t and z, and $\vec{P}^{(3)}_{NL}(\omega_a, t)$ is easily expressed in terms of the CARS susceptibility $\chi^{(3)}(\omega_a)$

$$P^{(3)}_{NL}(\omega_a,t) = \hat{e}\cdot\vec{P}^{(3)}_{NL}(\omega_a,t) = \chi^{(3)}(\omega_a)E_L^2E_S^* \times\exp i[(2k_L-k_S)z - (2\omega_L-\omega_S)t] + \text{c.c.} , \tag{6}$$

For simplicity one retains only the terms with the Raman resonance denominator $\omega_{ba} - \omega_L + \omega_S \simeq 0$ in the third-order perturbation expansion of $\rho(t)$. These terms give the Raman contribution χ_R to the CARS susceptibility, while the others, which are not calculated here, are small, frequency independent, and can be lumped together in the nonresonant susceptibility χ_{NR}. Including several possible Raman transitions of the molecules one gets

$$\chi^{(3)}(\omega_a) = \chi_{NR} + \sum_{a,b}\chi^{ba}_R . \tag{7}$$

Here, χ^{ba}_R is the Raman susceptibility associated with the Raman transition of frequency ω_{ba}

$$\chi^{ba}_R = \frac{N}{\hbar^3}\frac{1}{(\omega_{ba}-\omega_L+\omega_S-i\Gamma_{ba})}\left\{\sum_{n'}\left(\frac{\mu_{an'}\mu_{n'b}}{\omega_{n'a}-\omega_a-i\Gamma_{n'a}} + \frac{\mu_{an'}\mu_{n'b}}{\omega_{n'b}+\omega_a+i\Gamma_{n'b}}\right)\right.$$
$$\times\sum_n(\rho^{(0)}_{aa}-\rho^{(0)}_{nn})\left(\frac{\mu_{bn}\mu_{na}}{\omega_{na}+\omega_S-i\Gamma_{na}} + \frac{\mu_{bn}\mu_{na}}{\omega_{na}-\omega_L-i\Gamma_{na}}\right)$$
$$-\sum_{n'}\left(\frac{\mu_{an'}\mu_{n'b}}{\omega_{n'a}-\omega_a-i\Gamma_{n'a}} + \frac{\mu_{an'}\mu_{n'b}}{\omega_{n'b}+\omega_a+i\Gamma_{n'b}}\right)$$
$$\left.\times\sum_n(\rho^{(0)}_{bb}-\rho^{(0)}_{nn})\left(\frac{\mu_{bn}\mu_{na}}{\omega_{nb}-\omega_S+i\Gamma_{nb}} + \frac{\mu_{bn}\mu_{na}}{\omega_{nb}+\omega_L+i\Gamma_{nb}}\right)\right\} , \tag{8}$$

which we write

$$\chi_R^{ba} = (A+B)(\beta+\alpha) - (C+D)(\gamma+\delta) , \quad (9)$$

with $\mu_{an} = \langle a| \vec{P} \cdot \hat{e} |n\rangle$ the matrix component of the dipole moment operator $\vec{P}$; $|n\rangle$, $|a\rangle$, $|b\rangle$ discrete eigenstates of the molecules ($|n\rangle$ excited electronic state, $|a\rangle$ and $|b\rangle$ vibrational states coupled by the Raman transition of shift ω_{ba}); ω_{na} absorption frequencies with damping Γ_{na}; $N\rho_{aa}^{(0)}$, $N\rho_{bb}^{(0)}$, $N\rho_{nn}^{(0)}$ initial number densities of molecules in states $|a\rangle$, $|b\rangle$, and $|n\rangle$. $\rho_{nn}^{(0)}$ is in general negligible with respect to $\rho_{aa}^{(0)}$ and $\rho_{bb}^{(0)}$; however it can become large if the medium is exposed to electrical discharges or resonant radiation. Furthermore, higher-order corrections may have to be applied to these initial population factors due to saturation of some transitions by the pump waves (see Sec. III C 3).

In mixtures, χ_{NR} is contributed both by the probed molecules and by the non-Raman-resonant molecular species (diluent molecules). It is composed of terms analogous to those of χ_R^{ba}, but with nonresonant two-photon sum or difference denominators in place of the Raman resonance denominator. In the usual case where the number density N of the probed molecules is small compared to that of the diluent molecules, χ_{NR} is mainly contributed by the latter and is therefore a frequency-independent real number (provided that there are no one- or two-photon electronic resonances in the diluent molecules). However, some of the two-photon nonvibrationally resonant (NVR) terms contributed by the probed molecules, although small, also depend strongly upon the field frequencies in resonant CARS; they therefore should be included in χ_R^{ba} rather than left in χ_{NR}. As will be shown in Sec. II B 3, they can be combined with some of the terms in expression (8) of χ_R^{ba} under certain assumptions on collisional mechanisms, leading to the more widely used expression found in Refs. 19, 25–27, and 29.

B. Diagrammatic representation

Nonlinear optical susceptibilities have usually been obtained from density operator calculations by perturbation theory up to the desired order. The calculation of any specified order of the density operator involves the evaluation of a number of terms, each associated with a specific time sequence of perturbations to the wave function $|\psi\rangle$ and its complex conjugate $\langle\psi|$. The time ordering of the perturbations to $|\psi\rangle$ with respect to those to $\langle\psi|$ is important in the case of non-negligible homogeneous broadening. It arises since the density operator is then a statistical average of the product of the wave function and its complex conjugate, which undergo different evolutions in general.[30–33] Each of these time sequences can be depicted by means of a Feynman-type time-ordered diagram as discussed recently in Refs. 21, 22, and 33. Any diagram is made of two parts, as can be seen on those of Figs. 1–3 which we shall use below to visualize and calculate the main contributions to $\chi^{(3)}(\omega_a)$: on the left-hand side is plotted the time evolution of $|\psi\rangle$, and on the right-hand side that of $\langle\psi|$, so that one can follow the time evolution of the density operator contribution along the time axis (vertical axis).

Diagrams have been first utilized by Feynman[34] for the calculation of light scattering cross sections, in the limit of negligible lifetime and collisional broadening. In this limit the perturbations occuring on the wave function are strictly decoupled from those occuring on its complex conjugate and can be calculated independently. Then it is sufficient to visualize and calculate the time evolution of $|\psi\rangle$ only (Feynman diagrams). Diagrams have also been utilized for calculations of transition rates[31,32] in spontaneous scattering and recently for the calculation of TPA contribution to third-order nonlinear susceptibility.[33] There are several advantages to using the diagrammatic representation. The calculation of the density-matrix elements contributing to $P_{NL}^{(3)}(\omega_a, t)$ can be done directly by means of simple rules and without calculating lower-order terms. The diagrams also permit one to visualize and interpret the process associated with each term in $P_{NL}^{(3)}(\omega_a, t)$ better than

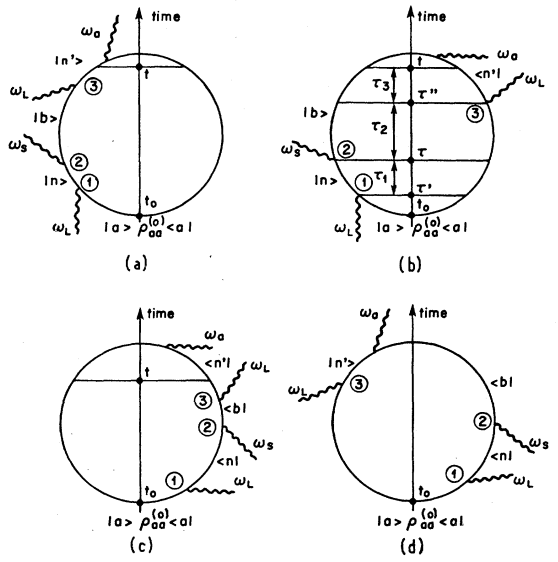

FIG. 1. Diagrammatic representation of the main contributions to $\chi^{(3)}(\omega_a)$ from molecules initially in state $|a\rangle$ (a) and (b) Raman resonant contribution; (c) and (d) Raman antiresonant contribution; (a) and (c) parametric diagrams; (b) and (d) nonparametric diagrams.

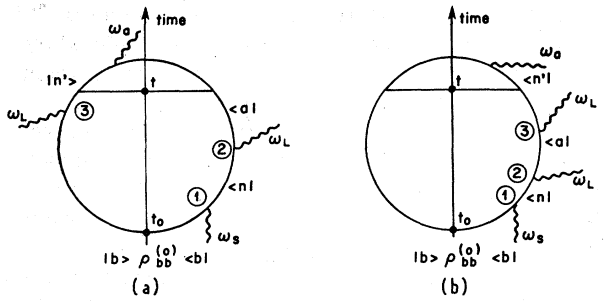

FIG. 2. Diagrammatic representation of the main contributions to χ_R proportional to $\rho^{(0)}_{bb}$. (a) nonparametric diagram; (b) parametric diagram.

do energy-level diagrams, which have brought much confusion concerning the parametric nature of CARS.

1. Diagrammatic analysis of $\chi^{(3)}(\omega_a)$

Each term of the CARS susceptibility is depicted by a time-ordered diagram representing the evolution of a density-matrix element as a function of time (the main ones are those shown in Figs. 1 and 2). The rules allowing one to specify the time-ordered diagrams and to directly evaluate the terms respectively associated with them have been stated in Refs. 21 and 22 and in Appendix A.

The contribution to $\chi^{(3)}(\omega_a)$ from the molecules initially in vibrational state $|a\rangle$ can be ascertained by considering the four basic diagrams of Fig. 1. The terms associated with Figs. 1(a) and 1(b) have a two-photon vibrational resonance (Raman resonance) denominator $(\omega_{ba} - \omega_L + \omega_S - i\Gamma_{ba})$, whereas those of Figs. 1(c) and 1(d) are Raman antiresonant $(\omega_{ba} + \omega_L - \omega_S + i\Gamma_{ba})$ and hence are smaller. We can associate two more time-ordered diagrams to each of the two initial diagrams of Figs. 1(b) and 1(d) as vertex 3 can occur before vertex 1 or between vertices 1 and 2; these new possibilities give terms possessing a two-photon sum or difference resonance instead of the vibrational Raman resonance. Each of these resultant eight fundamental diagrams gives another one by interchanging vertices 1 and 2, since emission at ω_S can occur before absorption at ω_L. On the eight fundamental diagrams, vertices 2 and 3 can also be interchanged, thus providing the last eight terms in χ_{NR}. The diagrammatic analysis thus indicates that there are 24 density-matrix terms proportional to the initial population factor $\rho^{(0)}_{aa}$ contributing to $\chi^{(3)}(\omega_a)$, four of which are vibrationally resonant. If the three pump waves had distinct frequencies ω_L, $\omega_{L'}$, ω_S (four wave mixing), there would be 48 terms.[35] The complete analysis shows that there are as many terms proportional to $\rho^{(0)}_{bb}$, and twice as many to $\rho^{(0)}_{mm}$ whose contributions subtract from the $\rho^{(0)}_{aa}$ and $\rho^{(0)}_{bb}$ terms. Some of the diagrams associated with the terms proportional to $\rho^{(0)}_{bb}$ are shown in Figs. 2 and 3.

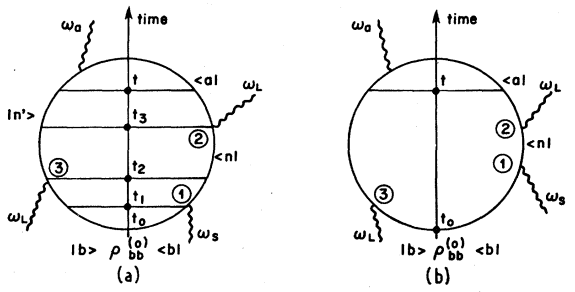

FIG. 3. Time-ordered diagrams derived from Fig. 2(a) with vertex 3 occuring: (a) between vertices 1 and 2; (b) before vertex 1.

2. On the parametric nature of CARS

CARS has frequently been represented by means of energy level diagrams. Such diagrams are commonly used in nonlinear optics to depict the creation of polarization by the applied fields, i.e., precisely for the role assigned to time-ordered diagrams in this paper. Energy-level diagrams can also be used to represent energy transfer between optical and vibrational modes; this has been their application to depict spontaneous processes like fluorescence or Raman scattering. We have adopted this interpretation for CARS below electronic resonances.[18,19] It is established that there are two distinct channels of energy flow[36] and thus two distinct types of diagrams are needed. The first one [Fig. 4(a)] stands for a process by which, on the average, two laser photons are converted into a Stokes and an anti-Stokes photon (the reverse process also being possible, depending on phase matching), so that there is no energy exchange between the fields and the molecules. The second diagram can be described as the interference of the Raman processes [Fig. 4(b)] operating between states $|a\rangle$ and $|b\rangle$; here too, the phases of the waves play a key role in determining the sense and magnitude of energy exchange.[24] If phase matching is satisfied and if

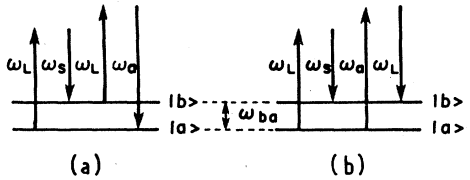

FIG. 4. Energy levels implied in CARS off resonance. (a) parametric process; (b) nonparametric process.

the anti-Stokes field is zero at the input boundary,[36] then a photon at ω_S is converted into a photon at ω_a and two vibrational quanta are extracted from the medium by this process, the rate being proportional to $|\mathrm{Im}\chi^{(3)}|^2$; the rate for the process of Fig. 4(a) is proportional to $|\mathrm{Re}\chi^{(3)}|^2$ under these conditions (see Ref. 19 and Appendix B). Both processes are subject to phase matching; that of Fig. 4(a), which in addition does not involve energy exchange with the medium, is truly parametric, whereas the other is not fully parametric and also possesses Raman character. When the field frequencies approach an electronic resonance, this is no longer valid and these diagrams do not fully represent the energy exchange involved in CARS.[37]

In short, the representation of energy transfers in CARS by means of energy-level diagrams is far from accurate, and similarly for the representation of the CARS polarization which is done usually by Fig. 4(a). Concerning the creation of the CARS polarization, time-ordered diagrams are superior. Each of these diagrams describes a quantum-mechanical sequence of interactions contributing to the creation of this polarization, together with the population changes subsequent to the interaction with the field at ω_a.

These diagrams actually are of two types. In the first ones [Figs. 1(a) and 2(b)], the interactions occur solely on one side (that is, either on the wave function or on its complex conjugate) while the other side remains unperturbed during the scattering. As a consequence, these processes cannot be accounted for by an amplitude squared transition probability. For simplicity we shall call these diagrams "parametric" because they describe the probability for the molecules to be returned to their initial state after the complete succession of interactions. The other type of diagram [Figs. 1(b) and 2(a)] gives the probability for the molecule initially in state $|a\rangle$ (or $|b\rangle$) to attain state $|b\rangle$ (or $|a\rangle$) and involves two interactions on each side of the diagram. We shall therefore call them nonparametric or Raman-type diagrams. If the wave function and its complex conjugate both interact with fields of identical frequencies (as happens in RS) the processes associated with a nonparametric diagram can be calculated from an amplitude squared transition probability. When certain simplifying assumptions on collisions are made (see Sec. II B 3), this calculation leads to Fermi's Golden Rule.

In conclusion one can readily calculate each term in $\chi^{(3)}(\omega_a)$ and associate it with the appropriate physical process by means of the diagrammatic representation. In particular, the Raman vibrationally resonant (RVR) terms in expression (8) of χ_R^{ba} are thereby easily visualized. Term $A\alpha$ is calculated from Fig. 1(a); it corresponds to a parametric diagram like term $D\gamma$ depicted in Fig. 2(b). Terms $B\alpha$ and $C\gamma$ are shown, respectively, in Figs. 1(b) and 2(a) and correspond to a nonparametric diagram. The last four terms $A\beta$, $B\beta$, $C\delta$, $D\delta$ are obtained from the diagrams of Figs. 1(a), 1(b) and 2 by interchanging vertices 1 and 2.

3. *Spectral distortions due to NVR time-ordered terms*

We shall now show that some of the two-photon NVR terms contributed by the Raman resonant species are more correctly included in the expression of χ_R rather than being left with χ_{NR}; they result indeed in a correction factor in expression (8) of χ_R which might be of importance in the case of resonant CARS. Similar corrections within χ_{NR} were discussed by Lynch *et al.*[35] Let us consider for instance the diagram of Fig. 2(a) and the two derived from it and shown in Fig. 3. These diagrams correspond in fact to different time orderings of the perturbation on the ket with respect to those on the bra. Combining the three associated terms, one obtains

$$B=\sum_{n,n'}-\rho_{bb}^{(0)}\frac{\mu_{an'}\mu_{n'b}\mu_{bn}\mu_{na}}{(\omega_{n'a}-\omega_a-i\Gamma_{n'a})}\left[\frac{1}{\omega_{ba}-\omega_L+\omega_S-i\Gamma_{ba}}\frac{1}{\omega_{nb}-\omega_S+i\Gamma_{nb}}\right.$$
$$\left.+\frac{1}{\omega_{nn'}+\omega_L-\omega_S+i\Gamma_{nn'}}\left(\frac{-1}{\omega_{nb}-\omega_S+i\Gamma_{nb}}+\frac{1}{\omega_{n'b}-\omega_L-i\Gamma_{n'b}}\right)\right]. \quad (10)$$

We now make the following approximation:

$$\Gamma_{nb}+\Gamma_{bn'}=\Gamma_{na}+\Gamma_{an'}=\Gamma_{nn'}\,, \quad (11)$$

which we shall refer to as damping approximation (11); the latter is satisfied if there is no elastic broadening and if the lifetimes of states $|a\rangle$ and $|b\rangle$ are much longer than those of $|n\rangle$ and $|n'\rangle$. Then (10) simplifies to

$$B=\sum_{nn'}-\rho_{bb}^{(0)}\frac{\mu_{an'}\mu_{n'b}\mu_{bn}\mu_{na}}{\omega_{ba}-\omega_L+\omega_S-i\Gamma_{ba}}\frac{1}{\omega_{n'b}-\omega_L-i\Gamma_{n'b}}$$
$$\times\frac{1}{\omega_{nb}-\omega_S+i\Gamma_{nb}} \quad (12)$$

One can see from (8) and (12) that the contributions of the two NVR terms depicted in Fig. 3 result in a shift of the electronic resonance of the RVR term

$C\gamma$ of Fig. 2(a) from $(\omega_{n'a}-\omega_a-i\Gamma_{n'a})$ to $(\omega_{n'b}-\omega_L-i\Gamma_{n'b})$. The other two diagrams arising from Fig. 2(a) as well as the four diagrams from Fig. 1(b) result, respectively, in an identical shift in term $C\delta$ and a shift of the one-photon antiresonance denominators of $B\alpha$, $B\beta$ from $(\omega_{n'b}+\omega_a+i\Gamma_{n'b})$ to $(\omega_{n'a}+\omega_L+i\Gamma_{n'a})$. These shifts become significant near a single-photon electronic resonance resulting in a change in χ_R from (8) to the widely used expression found in Refs. 19, 25–27, and 29. However, the latter expression is correct only when the damping approximation (11) is valid. Thus, one can show that it results from a non-time-ordered calculation, as obtained by diagrammatically evaluating the evolution of the wave function and that of its complex conjugate separately and multiplying the results together (which assumes that the time ordering of the vertices on the ket side with respect to that on the bra side is irrelevant). It is only in the case of the damping approximation (11) above that the three time-ordered contributions sum to provide a decoupling of the distinct evolutions of the wave function and of its complex conjugate.[38] When probing a specific Raman line in a gas mixture at atmospheric pressure, the damping approximation (11) is usually not valid. In that case, these NVR contributions of the probed molecules provide correction terms which cannot simplify and must be added to expression (8) of χ_R in order to get a correct interpretation of resonant CARS data.

C. Resonance into a continuum

As will be seen in Sec. III, the distortion in resonant CARS spectra resulting from interfering nearby resonances and from absorption linewidth fluctuations can be reduced by tuning the field frequencies into an absorption continuum. Our previous density-matrix perturbation calculation of $\chi^{(3)}(\omega_a)$ cannot be used here, since the damping approximation (3) is only valid in the case of Lorentzian broadening. To extend the analysis to the continuum case, the density matrix must span the eigenstates of the Hamiltonian H_0 lying in the continuum along with the previous base of discrete eigenstates $|r\rangle$, so that the closure relationship is now

$$1=\int d\alpha\,|\alpha\rangle\langle\alpha|+\sum_r |r\rangle\langle r|\,. \tag{13}$$

The calculation of $\vec{\mathrm{P}}^{(3)}_{NL}(\omega_a,t)$ from the density matrix is ideally suited to a generalization of the propagator approaches.[22,32] This calculation offers a great deal of insight in cases for which the damping approximations (3) and (11) are not valid. It is also expected that a better physical understanding of these continuum transitions and of the joint density of states will be obtained by means of CARS experiments.

$\vec{\mathrm{P}}^{(3)}_{NL}(\omega_a,t)$ is thus obtained by expression (4), where the summation over discrete states $|m\rangle$ and $|n\rangle$ must be extended to the continuum eigenstates. The contribution of the molecules lying in their lower state $|a\rangle$ to $\vec{\mathrm{P}}^{(3)}_{NL}(\omega_a,t)$ can be written

$$\begin{aligned}\vec{\mathrm{P}}^{(3)}_{NL}(\omega_a,t)=NT_r\vec{\mathrm{P}}\{&U^{(3)}(t,t_0)|a\rangle\rho^{(0)}_{aa}\langle a|U^{+(0)}(t,t_0)+U^{(0)}(t,t_0)|a\rangle\rho^{(0)}_{aa}\langle a|U^{+(3)}(t,t_0)\\&+U^{(2)}(t,t_0)|a\rangle\rho^{(0)}_{aa}\langle a|U^{+(1)}(t,t_0)\\&+U^{(1)}(t,t_0)|a\rangle\rho^{(0)}_{aa}\langle a|U^{+(2)}(t,t_0)\}_{AV}\,,\end{aligned} \tag{14}$$

where AV denotes an average over the statistical parameters of the ensemble of molecules, $U^{(n)}(t,t_0)$ and $U^{+(n)}(t,t_0)$ are, respectively, the time-evolution operators of the ket and bra, evaluated to the nth order in the field amplitude. It is readily seen that the first two terms in (14) correspond to the parametric time-ordered diagrams and the last two to the nonparametric ones. We only consider here the contributions of interest in resonant CARS to $\vec{\mathrm{P}}^{(3)}_{NL}(\omega_a,t)$ which we write

$$\hat{e}\cdot\vec{\mathrm{P}}^{(3)}_{NL}(\omega_a,t)=N\rho^{(0)}_{aa}\,[S_a+S_b+P_{12}(S_a)+P_{12}(S_b)]+\text{c.c.}\,; \tag{15}$$

S_a is that depicted in Fig. 1(a); S_b corresponds to the three time-ordered possibilities for vertex 3 in Fig. 1(b); P_{12} is an operator interchanging vertices 1 and 2 in Figs. 1(a) and 1(b). As was seen in Sec. II B the question of whether the evolution of the wave function is decoupled or not from that of its complex conjugate (depending on the damping approximation made) arises in the calculations of S_b and $P_{12}(S_b)$. Here we introduce phenomenologically the collisional broadening in the shape of the absorption continuum (more precisely, in the joint density of states as will be seen below). This allows us to eliminate the averaging AV in (14) and to write $U^{(0)}_{(\tau)}=e^{-iH_0\tau}$. We have

$$S_b + P_{12}(S_b) = \iint dn'\, db \langle n'|\, \vec{\mathbf{P}}\cdot\hat{e}\,|b\rangle \left\langle b \right| \sum\ e^{-iH_0 t} \int_{t_0}^{t} d\tau e^{iH_0\tau} V(\tau) e^{-iH_0\tau} \times \int_{t_0}^{\tau} d\tau' e^{iH_0\tau'} V(\tau') e^{-iH_0\tau'} |a\rangle\langle a| \times \int_{t_0}^{t} d\tau'' e^{iH_0\tau''} V(\tau'') e^{-iH_0\tau''} e^{iH_0 t} \left| n' \right\rangle , \quad (16)$$

where the integration over n', b is taken over both the continuum and discrete states. The two interactions occuring on the ket $|a\rangle$ at times τ' and τ are time ordered ($t_0 < \tau' < \tau < t$); $\sum$ represents the sum of the three time-ordered possibilities for time τ'': (i) $\tau' < \tau < \tau''$; (ii) $\tau' < \tau'' < \tau$; (iii) $\tau'' < \tau' < \tau$.

For many experimental situations (mostly in liquids but also in gases) the absorption continuum can be considered as a broad Lorentzian; in that case, the calculation of the three time-ordered possibilities is performed precisely as in Sec. II B. However, in the more general case when one cannot make any hypothesis on the type of broadening mechanism occuring in the continuum, the three time-ordered calculations must be performed in terms of joint densities of states. As an example, we shall derive the RVR term $S_b^{(i)}$ depicted in Fig. 1(b) and corresponding to case (i). With $t_0 \to -\infty$ in order to extract the steady-state contribution, and using the new set of variables $\tau_1 = \tau - \tau'$, $\tau_2 = \tau'' - \tau$, $\tau_3 = t - \tau''$, we obtain

$$S_b^{(i)} = -E_L^2 E_S^* e^{-i\omega_a t} e^{i(2k_L - k_S)z} \iiint dn\, dn'\, db \langle n'|\, \vec{\mathbf{P}}\cdot\hat{e}\,|b\rangle \times \int_{\infty}^{0} d\tau_1 \langle n|\, -\vec{\mathbf{P}}\cdot\hat{e}\,|a\rangle e^{-i(\omega_{na} - \omega_L)\tau_1} \int_{\infty}^{0} d\tau_2 \langle b|\, -\vec{\mathbf{P}}\cdot\hat{e}\,|n\rangle\, e^{-i(\omega_{ba} - \omega_L + \omega_S)\tau_2} \times \int_{\infty}^{0} d\tau_3 \langle a|\, -\vec{\mathbf{P}}\cdot\hat{e}\,|n'\rangle\, e^{-i(\omega_{bn'} - \omega_a)\tau_3} , \quad (17)$$

Changing from the set of independent variables n, b, n' to the set of independent variables ω_{na}, ω_{ba}, $\omega_{n'b}$ one has $dn' = d\omega_{n'b}\, g(\omega_{n'b})$; $dn = d\omega_{na}\, g(\omega_{na})$; $db = d\omega_{ba}\, g(\omega_{ba})$, where $g(\omega_{nn'})$ is the joint density of states associated with the transition frequency $\omega_{nn'}$. Taking a Lorentzian distribution for the joint density of states $g(\omega_{ba})$ associated with the Raman vibrational frequency ω_{ba}, i.e.,

$$g(\omega_{ba}) = \Gamma_{ba}^2 / \pi[(\omega_{ba} - \omega_L + \omega_S)^2 + \Gamma_{ba}^2] , \quad (18)$$

one gets

$$S_b^{(i)} = -e^{-i\omega_a t} e^{i(2k_L - k_S)z} \int d\omega_{na}\, g(\omega_{na}) \langle n|\, -\vec{\mathbf{P}}\cdot\hat{e}\,|a\rangle \left(\pi\delta(\omega_{na} - \omega_L) - i\mathcal{P}\, \frac{1}{\omega_{na} - \omega_L} \right) \times \int d\omega_{bn'} g(\omega_{bn'}) \langle a|\, -\vec{\mathbf{P}}\cdot\hat{e}\,|n'\rangle \left(\pi\delta(\omega_{bn'} - \omega_a) - i\mathcal{P}\, \frac{1}{\omega_{bn'} - \omega_a} \right) \frac{\langle b|\, -\vec{\mathbf{P}}\cdot\hat{e}\,|n\rangle\langle n'|\, \vec{\mathbf{P}}\cdot\hat{e}\,|b\rangle}{(\omega_{ba} - \omega_L + \omega_S - i\Gamma_{ba})} E_L^2 E_S^* \quad (19)$$

where δ is the Dirac function and $\mathcal{P}$ the principal value operator. Similarly, S_a, $S_b^{(ii)}$, and $S_b^{(iii)}$ can be evaluated from the associated diagrams or can be directly inferred from the terms obtained in the discrete case by writing

$$\sum_{kk'} \frac{1}{\omega_{kk'} - \omega \pm i\Gamma_{kk'}} = \int d\omega_{kk'}\, g(\omega_{kk'}) \left(\mp i\pi\delta(\omega_{kk'} - \omega) + i\mathcal{P}\, \frac{1}{\omega_{kk'} - \omega} \right) , \quad (20)$$

for any k and (or) k' referring to a continuum state. The broadening mechanism is included in the joint density of states $g(\omega_{kk'})$. Thus, if no assumption is made on $g(\omega_{kk'})$, the three time-ordered possibilities $S_b^{(i)}$, $S_b^{(ii)}$, $S_b^{(iii)}$ cannot be summed into a simple non-time-ordered result.[39] In fact, we note that the three contributions $S_b^{(i)}$, $S_b^{(ii)}$, $S_b^{(iii)}$ can be expressed in terms of joint densities of states, respectively, associated with specific transitions only if the interaction $V(\tau'')$ on the bra is specifically time-ordered with respect to the set of interactions $V(\tau)$, $V(\tau')$ on the ket. Of course, molecules in

the upper vibrational state would give an analogous contribution to $\vec{P}^{(3)}_{NL}(\omega_a, t)$ but proportional to $\rho^{(0)}_{bb}$.

Resonance continuum excitation of RRS has been studied theoretically and experimentally.[40-42] It is of interest to consider the analogy of (15)–(19) with the expression of the RRS cross section, which is given by[40]

$$\frac{d\sigma}{d\Omega} = \frac{\omega_L \omega_S^3}{c^4 \hbar^2} \left| \sum_n \left\{ \frac{\mu_{bn}\mu_{na}}{\omega_{na} - \omega_L - i\Gamma_{na}} + \frac{\mu_{bn}\mu_{na}}{\omega_{nb} + \omega_L - i\Gamma_{nb}} \right\} + i\pi \mu_{b\alpha_L} \mu_{\alpha_L a} \rho_\alpha(\omega_L) + \mathcal{P} \int_{D_e/\hbar}^{\infty} d\omega_\alpha \rho_\alpha(\omega_\alpha) \frac{\mu_{b\alpha}\mu_{\alpha a}}{\omega_{\alpha a} - \omega_L} + \int_{D_e/\hbar}^{\infty} d\omega_\alpha \rho_\alpha(\omega_\alpha) \frac{\mu_{b\alpha}\mu_{\alpha a}}{\omega_{\alpha b} + \omega_L} \right|^2$$

$$= \frac{\omega_L \omega_S^3}{c^4 \hbar^2} |A + B + C + D|^2 , \qquad (21)$$

where $\rho_\alpha(\omega_a)$ is defined as the density of continuum states of energy $\hbar\omega_\alpha$ above the initial state $|a\rangle$. Calculations carried out in Refs. 40 and 41 have demonstrated that the contribution A (in curly brackets) of discrete states close to the dissociative limit D_e, the contribution $B = i\pi\mu_{b\alpha_L}\mu_{\alpha_L a}\rho_\alpha(\omega_L)$ of state $|\alpha_L\rangle$ resonant with the laser frequency ω_L, the principal value contribution C, and the antiresonant contribution D can be of equal importance and can interfere with each other. This is easily understood by visualizing the continuum as a broad Lorentzian line of width Γ; then, as long as the detunings $(\omega_{\alpha a} - \omega_L)$ and $(\omega_{na} - \omega_L)$ of the off-resonant electronic states are of the order of Γ, these states give a contribution equivalent to that of state $|\alpha_L\rangle$. It is apparent from (15)–(19) that the CARS susceptibility can be expressed in terms of contributions having the same form as A, B, C but with slightly different transition moments and energy denominators. The NVR time-ordered contributions $S_b^{(ii)}$, $S_b^{(iii)}$, $P_{12}(S_b^{(ii)})$, $P_{12}(S_b^{(iii)})$ can be written $(A_1+B_1+C_1+D_1)\times(A_2+B_2+C_2+D_2)\times(A_3+B_3+C_3+D_3)$ whereas the RVR time-ordered contributions S_a, $S_b^{(i)}$, $P_{12}(S_a)$, $P_{12}(S_b^{(i)})$ can be written in the form $(A_1+B_1+C_1+D_1)\times(A_2+B_2+C_2+D_2)\times 1/(\omega_{ba} - \omega_L + \omega_S - i\Gamma_{ba})$ where B_i comes from the integration of the δ function, C_i from the principal value integration, and A_i corresponds to the contribution of discrete eigenstates close to the dissociative limit which must be added in (19). In contrast to these expressions, Eq. (21) involves a squared amplitude resulting from a non-time-ordered calculation. As discussed above, this is an approximation and should be replaced, to be strictly correct, by the three time-ordered contributions associated with the Raman effect.[21,22] As a consequence $\rho_\alpha(\omega_\alpha)$ in (21) is analogous to joint densities of states in which one state is the initial state $|a\rangle$. However, it is expected that the difference between the non-time-ordered and the time-ordered calculations will not be as important in the case of a broad absorption line (continuum) as for that of an isolated sharp absorption line. In any case, the basic approach used in Ref. 40 for the numerical calculation of A, B, C, D is directly applicable in the present case.

In conclusion, when one can approximate the continuum as a broad Lorentzian line, a non-time-ordered calculation seems sufficient to estimate the main characteristics of resonant CARS by comparison with experimental results obtained in RRS; in particular the variation of χ_R with the field frequencies should be smoother than in the case of discrete electronic resonance. It is furthermore expected that CARS investigations within the continuum, when interpreted by means of the rigorous time-ordered calculation, will contribute to an understanding of continuum transitions.

III. SPECTRA IN RESONANT CARS AND APPLICATIONS

Conventional CARS spectra produce essentially the same spectral features as those found in normal RS spectra. In particular, CARS has permitted the observation of the familiar O, Q, and S branches in gaseous H_2 and N_2.[5,18] There are, however, two key differences in the spectra obtained from the two techniques. Firstly, the line strengths differ by a population factor; secondly, the line contours are markedly different in CARS as a result of complex interferences between neighboring Raman lines and the nonresonant background. These interferences also limit the detectivity of CARS.[18]

When electronic resonance enhancements are sought for, two distinct cases must be considered: resonance with discrete absorption lines or with a continuum [Figs. 5(a) and 5(b)]. In both cases, the CARS spectra will present new characteristics, particularly with regards to spectral content, line strengths, shifts, and contours. We shall examine them in turn. We shall also study the influence upon absorption linewidths of fluctuations in density and temperature occuring in unstable media. Fin-

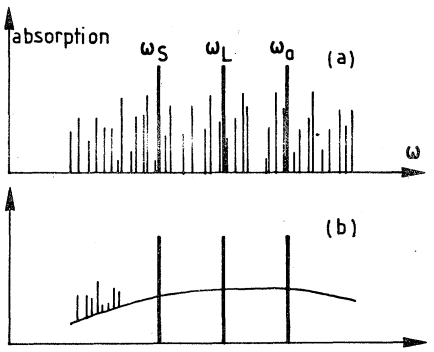

FIG. 5. Spectral configurations for CARS resonance enhancement: (a) with discrete lines; (b) with a continuum.

ally, the detectivity improvement obtained in each type of resonant excitation will be estimated. The discussion will be centered on the gas phase, which presents a somewhat more complex picture than liquids. We shall, however, outline some of the properties of the latter in the light of recent experimental work.

A. Spectral content

Several authors have examined the selection rules for conventional CARS and concluded that they are the same as for normal RS.[43,44] Therefore, the same Raman resonances are found in either type of spectra, although they differ in strength by the population factor. In CARS, when the light frequencies are all well below the absorption frequencies, the electronic terms multiplying $\rho_{aa}^{(0)}$ and $\rho_{bb}^{(0)}$ are nearly equal, so that $\rho_{aa}^{(0)} - \rho_{bb}^{(0)}$ factors out. Therefore, the intensity of the Raman resonance is proportional to $\rho_{aa}^{(0)} - \rho_{bb}^{(0)}$, in contrast to RS for which proportionality to $\rho_{aa}^{(0)}$ is observed. This difference is minor in general for vibrational spectra if the temperature is low, but is always considerable for pure rotational spectra because the populations in states $|a\rangle$ and $|b\rangle$ are nearly equal (this property will partially offset the gains in cross section and detectivity one expects in going from vibrational to rotational transitions).

1. Resonance with discrete absorption lines

From (8) and (12), one can see that χ_R shows resonant enhancement whenever ω_a, ω_L, or ω_S come close to a discrete absorption frequency. Thus, the CARS spectrum may present a complex structure, since any of these three frequencies may come into resonance with absorption lines as the vibrational-rotational structure is being analyzed. Only the levels associated with these one-photon transitions will contribute strongly, so that the spectrum will be very different from the off-resonance case. Moreover, the contribution of the population factor $\rho_{aa}^{(0)}$ in χ_R is no longer equal to that of $\rho_{bb}^{(0)}$ and their respective weights vary differently as the spectrum is scanned. However, simplifications will occur, since (i) One of the three frequencies (ω_L in general) is usually held fixed in resonance with an absorption line for instrumental convenience. (ii) When the Raman spectrum is analyzed, $\omega_L - \omega_S$ is varied over a finite spectral domain and a limited number of Raman transitions contribute to the susceptibility. For a given Raman transition i from $|a^i\rangle$ to $|b^i\rangle$, there are only two types of allowed one-photon transitions to or from each of the rotational sublevels $|a^i\rangle$, $|b^i\rangle$, i.e., $\Delta J = \pm 1$; therefore the number of absorption lines that ω_S or ω_a can reach to enhance χ_R is finite. (iii) One can often assume $T_v \ll \hbar\omega_{ba}/k$ where T_v is the vibrational temperature and k the Boltzmann constant, so that $\rho_{bb}^{(0)} \ll \rho_{aa}^{(0)}$. Similarly, $\rho_{nn}^{(0)} \ll \rho_{aa}^{(0)}$, $\rho_{bb}^{(0)}$. (iv) Then, only term $A\alpha$ in Eq. (9) is large, the other electronic terms containing antiresonance denominators.

For these conditions, disregarding all electronic terms but $A\alpha$, we will show that the dominant characteristics are provided by double resonances: these involve combinations of any two of the three following resonances, i.e., vibrational on ω_{ba}, electronic with ω_L tuned on ω_{na} or with ω_a tuned on $\omega_{n'a}$; triple resonances are improbable because level spacings are different in the ground and excited electronic states.

As an example, let us consider the case of I_2 at low temperature (hence $\rho_{bb}^{(0)} = 0$). We shall seek resonance enhancement from one-photon transitions between the $X^1\Sigma_g^+$ state, whose vibration-rotation manifold contains all the $|a\rangle$ sublevels, and the upper state $B^3\pi_{ou}^+$ which contains the $|n\rangle$ sublevels. If ω_L is tuned to a particular, isolated, absorption line ω_{na^i}, one selects the particular and unique initial state, which we label $|a^i\rangle = (v'', J)$, among all the possible $|a\rangle$ sublevels. Selection rules prescribe $J' = J \pm 1$ for $|n\rangle$, which shall be labeled (v', J'). We shall discuss here the case of an R transition, i.e., $J' = J + 1$ (Fig. 6). One then observes, as ω_S is varied, omitting the i superscript in the molecular frequencies:

(a) $(\omega_{na}, \omega_{ba})$ double resonances, i.e., $\omega_L = \omega_{na}$ and $\omega_L - \omega_S = \omega_{ba}$ [Fig. 6(a)]. These are made up of fundamental and overtone Raman doublets with spacings equal to those of the various vibrational states in the electronic ground state [Fig. 7(a)]. The doublets are composed of one Q and one S Raman line if ω_L is resonant with an R absorption line (or of an O and a Q line if the absorption line is a P line). These resonances obviously correspond to the allowed Raman transitions originating from level $|a^i\rangle$.

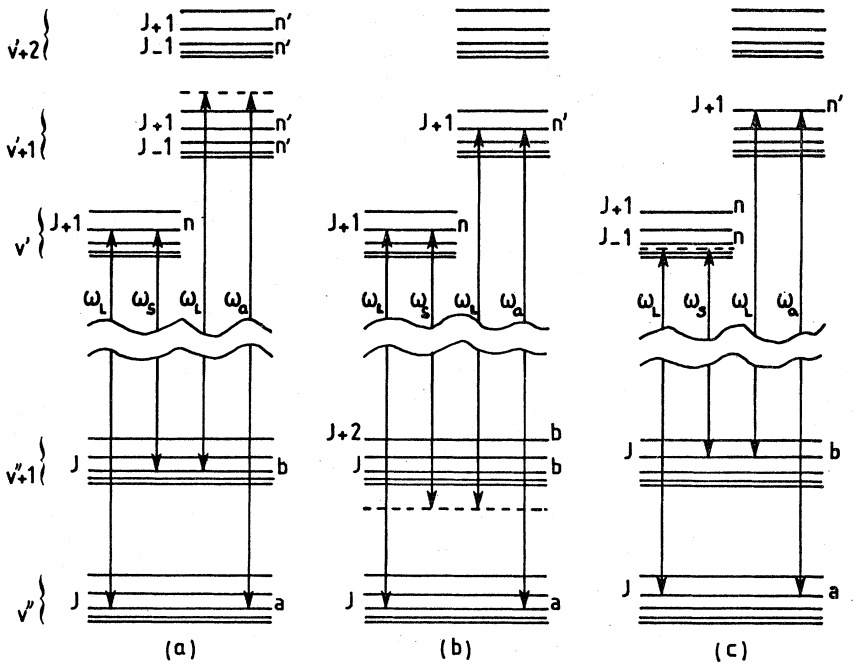

FIG. 6. Energy level diagrams representing the states contributing to resonance-enhanced CARS in a diatomic molecule: (a) fundamental ($\Delta v = 1$) Raman vibrational resonance enhanced by the resonance condition $\omega_L = \omega_{na}$; (b) double electronic resonance with $\omega_L = \omega_{na}$ and $\omega_a = \omega_{n'a}$; (c) fundamental vibrational resonance enhanced by the resonance condition $\omega_a = \omega_{n'a}$. These diagrams must not be mistaken for those of Fig. 4, which represent the energy flow associated with CARS off resonance.

Doppler broadening on these lines is small for the same reason as in any CARS or spontaneous Raman scattering experiment in the forward direction.[12] If collisional broadening dominates, the strengths of these lines are inversely proportional to $\Gamma_{na}\Gamma_{ba}|\omega_a - \omega_{n'a}|$. When exact vibrational resonance is obtained ($\omega_L - \omega_S = \omega_{ba}$), ω_S is also automatically resonant with the allowed transition ω_{nb}. This resonance, however, only enters into the $C\gamma$ and $D\gamma$ terms, which possess negligible weight in χ_R because $\rho_{bb}^{(0)} \simeq 0$. Unless a fortuitous coincidence takes place, ω_a will not be simultaneously in exact resonance with the $\omega_{n'a}$ allowed transitions from $|a^i\rangle$ (triple resonance); actually, the detuning $\omega_{n'a} - \omega_a$ may be as large as 60 cm^{-1} in iodine, since the spacing between the vibrational sublevels is about 120 cm^{-1} in the $B\,^3\pi_{ou}^+$ state. If a second pump laser at $\omega_{L'}$ were used, then the frequency $\omega_a = \omega_L + \omega_{L'} - \omega_S$ could be tuned independently to one of the $\omega_{n'a}$ resonances, giving additional enhancement of the CARS line.

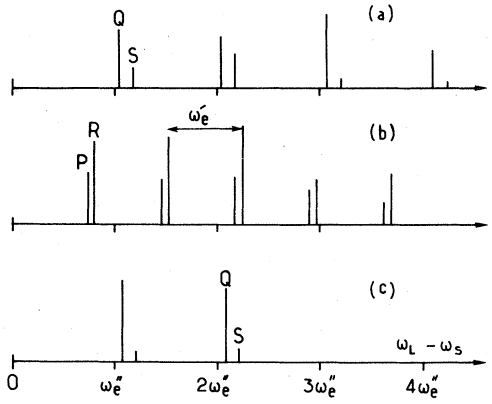

FIG. 7. Break up of the CARS spectrum into the three types of double resonances: (a) fundamental and overtone lines resulting from resonances of the type depicted in Fig. 6(a). Doublet spacing is constant (if anharmonicity is neglected) and is equal to ω_e''. (b) doublets associated with Fig. 6(b) (spacing is ω_e'). (c) doublets associated with Fig. 6(c), assuming $|b\rangle$ is in the second excited vibrational level, so that only two doublets are seen. Here, spacing is ω_e'' but the lines do not coincide with those of Fig. 7(a) in general because J is different.

(b) $[\omega_{na}, \omega_{n'a}]$ double resonances [Fig. 6(b)]. These are made up of P and R lines occurring in doublets and corresponding to possible resonances between ω_a and the allowed one-photon transitions from $|a^i\rangle$. The positions of these lines in the spectrum are obtained from the condition $\omega_L - \omega_S = \omega_{n'a} - \omega_L$. The spacing between the doublets is equal to that between the vibrational levels in the excited electronic state [Fig. 7(b)]. The analysis of such lines is a new spectroscopy which can be of great importance for the precise study of one-photon absorption. If collisional broadening dominates, their strengths are inversely proportional to $\Gamma_{na}\Gamma_{n'a}|\omega_{ba} - \omega_L + \omega_S|$. Their intensities are comparable to those of the Raman lines discussed in (a). One can also by this technique select and analyze any weak $\omega_{n'a}$ resonance buried in a continuum by simply tuning ω_L to one of the other allowed but strong ω_{na} absorptions originating from $|a^i\rangle$.

(c) In addition to these two families of double resonances associated with level $|a^i\rangle$, one also expects another class of double resonances namely $[\omega_{n'a}, \omega_{ba}]$

double resonances pertaining to a different initial level $|a^j\rangle$ [Fig. 6(c)]. The location of these resonances can easily be obtained if one realizes that for ω_a and $\omega_L - \omega_S$ to be simultaneously resonant, it is necessary for ω_L to also be resonant with the $\omega_{n'b}$ transitions. The latter usually do not appear in the absorption spectrum because $\rho_{bb}^{(0)} = 0$, but would of course be observed at higher temperatures. Identification of $|a^j\rangle$ immediately gives the doublets to be found ($O+Q$ for ω_L tuned to an R line, $Q+S$ for a P line) [Fig. 7(c)]. Doppler broadening is also small here. If collision broadening dominates, the line strengths are inversely proportional to $\Gamma_{n'a}\Gamma_{ba}|\omega_{na} - \omega_L|$.

(d) Whenever a resonance in Fig. 7(a) coincides with one in Fig. 7(b), one then has a triple resonance and the resulting intensity is strongly enhanced.

In brief, the complete spectrum corresponding to ω_L fixed to a given ω_{na} contains the two sets of doublets predicted in Figs. 7(a) and 7(b). If the absorption spectrum actually contains several other lines close to or coincident with ω_{na}, each of these will also contribute its two associated sets of doublets. Each one of the possible $\omega_{n'b} = \omega_L$ resonances, if any, will also contribute its associated set of doublets as depicted in Fig. 7(c). All these strong lines interfere with one another in the usual fashion.[18] Furthermore, they emerge on top of, and also interfere with, the rest of the O, Q, and S lines which are only weakly enhanced. Finally, the intensities of all these lines also depend on $\rho_{aa}^{(0)}$ and on the transition moments (see Sec. III C 1).

If the temperature is raised, the resonant CARS spectrum is complicated due to the contribution of the $\rho_{bb}^{(0)}$ terms. The main contribution from $\rho_{bb}^{(0)}$ actually comes from term $C\gamma$ in Eq. (9), which has one electronic resonance in common with $A\alpha$. In addition, one must take into account the two NVR terms in χ_{NR} which are time-ordered variations of $C\gamma$ and are given in Eq. (10). We have seen that these can change the character of the expected electronic resonances in $C\gamma$. In particular, if the damping approximation (11) is valid, the $\omega_{n'a} - \omega_a$ resonance denominator is replaced by $\omega_{n'b} - \omega_L$. If not, a still more complicated situation occurs since the $(\omega_{n'a} - \omega_a)$ pole in $C\gamma$ is then not exactly cancelled by the two NVR terms. Thus one can expect electronic resonant effects due to the three poles $(\omega_{n'a} - \omega_a)$, $(\omega_{n'b} - \omega_L)$ and $(\omega_{nb} - \omega_S)$. As a consequence, the main effects on the spectrum will be a change in the intensities of all the features associated with $\rho_{aa}^{(0)}$, together with a slight distortion of their contours. Consider for instance the set of Raman doublets corresponding to the double resonance $[\omega_{na}, \omega_{ba}]$ in term $A\alpha$. The lines are modified primarily by corrections from term $C\gamma$, which exhibits the double resonance $[\omega_{nb} \simeq \omega_S, \omega_{ba} \simeq \omega_L - \omega_S]$; one can show that the contribution of the NVR terms to these lines is negligible compared with that of $C\gamma$ (typically 1/100th that of $C\gamma$ for $\omega_{n'a} - \omega_a = 10\ \mathrm{cm}^{-1}$ and linewidths of $0.1\ \mathrm{cm}^{-1}$). For the other two sets of doublets, namely vibrational $[\omega_{n'a}, \omega_{ba}]$ and double electronic $[\omega_{na}, \omega_{n'a}]$, $C\gamma$ and the NVR terms give corrections of comparable magnitude. For the vibrational set, the $[\omega_{n'a}, \omega_{ba}]$ double resonance in $C\gamma$ is of similar amplitude as the $[\omega_{n'a} \simeq \omega_a, \omega_{n'b} \simeq \omega_L]$ double resonance appearing in the NVR terms. For the electronic set, one has, for a detuning $\omega_{n'a} - \omega_a = \epsilon$ from the line center, $\omega_{n'b} - \omega_L = \omega_{nb} - \omega_S - \epsilon$ and $\omega_{nn'} + \omega_L - \omega_S = \epsilon$, so that the two NVR terms can be combined to give a contribution of the form

$$\rho_{bb}^{(0)}(-\epsilon + i\Gamma_{nb} + i\Gamma_{n'b})[(\epsilon - i\Gamma_{nn'})(\omega_{n'a} - \omega_a - i\Gamma_{n'a}) \times (\omega_{nb} - \omega_S + i\Gamma_{nb}) \times (\omega_{n'b} - \omega_L - i\Gamma_{n'b})]^{-1}. \quad (22)$$

Obviously, this contribution and that from $C\gamma$ have the same pole at $\omega_{n'a}$. Furthermore, they almost cancel, and their sum is zero at line center ($\epsilon = 0$) if the damping approximation (11) is valid; the contribution of $\rho_{bb}^{(0)}$ to the electronic lines is therefore negligible with respect to that of $\rho_{aa}^{(0)}$, which is doubly resonant.

All these complications resulting from the $\rho_{bb}^{(0)}$ terms can of course be very severe for the fundamental band of I_2 at room temperature, hence the interest in performing the spectroscopy of the overtone bands of high rank (e.g., 4 and above), for which $\rho_{bb}^{(0)}$ is negligible. The experiments reported in Sec. V were carried out precisely under those conditions.

2. *Resonance with a dissociative continuum*

Tuning the pump frequencies into a continuum would eliminate the problems due to multiple interfering sharp resonances associated with the $\rho_{aa}^{(0)}$ and $\rho_{bb}^{(0)}$ terms. There are indeed many initial states $|a\rangle$ and intermediate states $|\alpha\rangle$ and $|r\rangle$ giving interfering equivalent contributions to χ_R, so that the dependence of $\chi^{(3)}(\omega_a)$ upon the field frequencies would be smoother. Resonance enhancement comes simultaneously from ω_L and ω_a. Furthermore, we anticipate the CARS spectrum to only contain the usual vibration-rotation features (and no longer the double electronic resonance features), constituting enhanced O, Q, and S branches having relative intensities similar to those encountered off-resonance.

B. Line contours

In addition to predicting the features in the CARS spectrum, one can also describe their spectral contour. The first experimental evidence of reso-

nance CARS has been reported recently for the liquid phase,[15,16] leading to the observation of unusual dispersive properties. Liquids differ markedly from gases because the molecules cannot rotate freely, and also because the absorption lines usually merge into a continuum. Therefore, the Raman resonance pertaining to a particular vibrational mode is unique (no rotational splitting) and is electronically enhanced as a whole.

An interpretation of the results of Ref. 16 was given recently by means of computer calculations.[28,45,46] A much simpler discussion can in fact be given by means of the circle model introduced in Refs. 18 and 19 for nonresonant CARS. This discussion will be presented in the context of chemical analysis, where one tries to detect the Raman resonances of the species of interest in the presence of a nonresonant background which is contributed by the diluent. We shall first present the circle model for the nonresonant case; the case of discrete absorption lines will then be considered. Finally, generalization to absorption continua will be performed.

The circle model was introduced when it was realized that the CARS spectrum is just a plot of the modulus of $\chi^{(3)}(\omega_a)$ vs ω_S, and that $\chi^{(3)}(\omega_a)$ can be represented as a vector in the complex plane. It was then found that the extremity of this vector $\vec{\chi}$ describes a circle during the spectral scan. As a matter of fact, $\vec{\chi}$ is the sum of two vectors, i.e. $\vec{\chi}_R$ whose argument and modulus depend upon ω_L, ω_S and ω_a, and $\vec{\chi}_{NR}$ which is a constant. The equation for the RVR part $\vec{\chi}_R$ associated with one particular Raman resonance ω_{ba} can be written

$$\chi_R = N\alpha_R/(\omega_{ba} - \omega_L + \omega_S - i\Gamma_{ba}) = X + iY \ , \qquad (23)$$

where N is the number density and α_R stands for electronic terms, population factors, etc. In the nonresonant case, α_R is a real number proportional to the RS cross section $d\sigma/d\Omega$ and to $\rho_{aa}^{(0)} - \rho_{bb}^{(0)}$; it depends little upon field frequencies and can be taken as a constant. Then the expression for χ_R can be interpreted as the parametric equation for two families of orthogonal circles (Fig. 8). The main family is described by $\vec{\chi}_R$ as $\omega_L - \omega_S$ is varied about ω_{ba} with the linewidth Γ_{ba} held fixed. There is a circle for each value of Γ_{ba}. The circle equation is $X^2 + (Y - 1/2y)^2 = (1/2y)^2$ with $y = \Gamma_{ba}/N\alpha_R$ as a parameter. For each particular experimental situation, only the circle with the relevant y parameter needs to be drawn. This circle is tangent to the X axis at the origin and lies in the upper half plane. Its diameter is y^{-1}. For a given detuning $\omega_{ba} - \omega_L + \omega_S$, the position of $\vec{\chi}_R$ on the preceding circle is found at the intersection with the orthogonal circle whose equation is $(X - 1/2x)^2 + Y^2 = (1/2x)^2$ with $x = (\omega_{ba} - \omega_L + \omega_S)/N\alpha_R$ as a parameter. There is a circle for each value of x, and these circles constitute the second family.

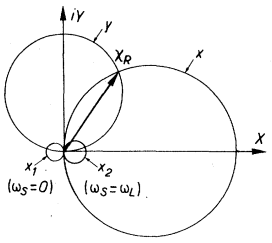

FIG. 8. Representation of χ_R as a vector in the complex plane. The extremity of this vector describes the circle of parameter y as the detuning x is being varied, and is found at the intersection with circle of parameter x. The vector tip is actually excluded from the small segment of arc contained within the circles of parameters $x_1 = (\omega_{ba} - \omega_L)/N\alpha_R$ and $x_2 = \omega_{ba}/N\alpha_R$.

It is seen readily that $\vec{\chi}_R$ rotates clockwise as ω_S is increased from $-\infty$ to $+\infty$; its argument decreases from π to 0 and is equal to $\frac{1}{2}\pi$ on resonance, i.e., at $\omega_S = \omega_L - \omega_{ba}$. In actuality, ω_S can only be varied from 0 to ω_L, so that a small segment of arc on either side of the origin is not swept. Adding χ_{NR} results in a translation parallel to the X axis [Fig. 9(a)]. The line contour is then drawn readily by plotting $|\vec{\chi}|$ as a function of x (or ω_S). If only an approximate line shape is to be rendered, it is sufficient to represent $\vec{\chi}_{NR}$ and the circle of parameter y on the diagram, from which the whole contour is directly pictured.

The line shape depends upon the relative magnitudes of y and χ_{NR} or, in other words, upon the mixing ratio N/N_d where N_d is the diluent density ($\chi_{NR} \propto N_d$). The case depicted in Fig. 9(a) corresponds to N/N_d large, i.e., $N/N_d \gg 1$ for typical molecular parameters and near STP. Apart from a slight asymmetry caused by the interference with χ_{NR}, the contour of $|\vec{\chi}|$ then closely fits the square root of a Lorentzian. In the other limit, if the concentration is small, the line contour approaches that of $\mathrm{Re}(\chi) = \chi_{NR} + X$, since Y gives a higher-order correction [Fig. 9(b)]. In either case, the difference between the maximum and the minimum is strictly equal to the magnitude of the vibrational resonance, i.e., one circle diameter $y^{-1} = N\alpha_R/\Gamma_{ba}$. This discussion describes accurately the case of isolated lines (e.g., Q lines in H_2, O, and S lines in N_2). For overlapping lines producing a non-Lorentzian contour (e.g., in a Q branch), the predictions of this model are still in qualitative agreement with the band shapes actually observed.[18]

When enhancement of χ_R through electronic resonances is produced, a complex situation appears since several of the terms in α_R can become large simultaneously and can vary as $(\omega_L - \omega_S)$ is varied. The discussion, however, remains simple for the

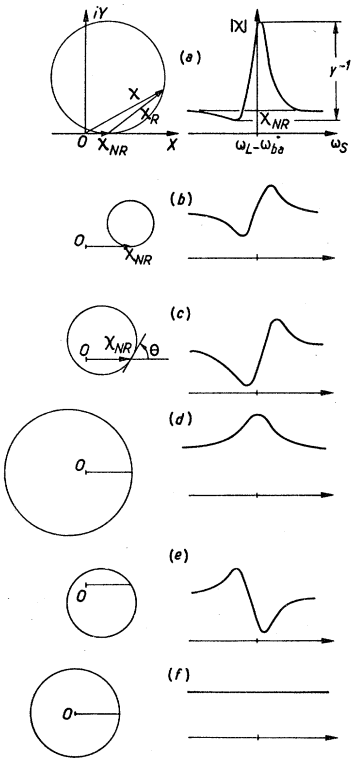

FIG. 9. Circle diagrams and corresponding line contours well below electronic resonances (a, b) and in vicinity of an electronic resonance (c–f), with $\mu_{an'}\mu_{n'b}\mu_{bn}\mu_{na}$ real. The circles and their parameters are defined in the text: (a) strong isolated Raman resonance ($N/N_d \geq 0.1$ typically); the circle described by $\vec{\chi}$ is represented, together with an approximate line contour displayed vs ω_S. (b) weak Raman resonance; only $\vec{\chi}_{NR}$ and the circle described by $\vec{\chi}_R$ are drawn on the diagram. (c) same as (b), but ω_L has been increased and tuned close to a one-photon resonance ω_{na}, with $\omega_L < \omega_{na}$; as a result the circle has been rotated and its diameter increased. (d) $\omega_L = \omega_{na}$; the circle diameter is at its maximum, and $\theta = \frac{1}{2}\pi$. (e) $\omega_L > \omega_{na}$; the diameter decreases again. (f) $\omega_L = \omega_{na}$, with the mixing ratio chosen such that the circle radius is equal to χ_{NR}; the line vanishes.

conditions assumed above in the presentation of the spectral content of $\chi^{(3)}(\omega_a)$ (i.e., $\rho_{bb}^{(0)}$ negligible, ω_L set near resonance, ω_a off resonance). Then, α_R is proportional to $\rho_{aa}^{(0)}$ and independent of ω_S and ω_a over the range of interest, and we can write

$$\alpha_R \propto \mu_{an'}\mu_{n'b}\mu_{bn}\mu_{na}/(\omega_{na} - \omega_L - i\Gamma_{na}) = \rho e^{i\theta}. \quad (24)$$

For ω_L fixed, it is apparent that $\vec{\chi}$ still describes the two families of circles. The circles are rotated by argument θ about the extremity of χ_{NR}, and their diameters scale as ρ. The rotation of the circles proceeds counterclockwise as ω_L increases past the one-photon resonance ω_{na}. If the product of transition moments is real, θ grows from 0° to 180° and is precisely 90° on resonance. Figures 9(c)–9(e) illustrate what happens to the circle of parameter y and the associated vibrational resonance of Fig. 9(b) assuming ω_L tuned slightly less than ω_{na}, to exactly ω_{na} and slightly greater than ω_{na}, respectively. Cases (c) and (e) produce line shapes which are mirror images of one another with respect to $\omega_S = \omega_L - \omega_{ba}$. Case (d) is interesting: depending on the magnitude of the Raman resonance with respect to χ_{NR}, the line, which is symmetrical with respect to $\omega_L - \omega_{ba}$ appears as a maximum [Fig. 9(d)] or a minimum, or even vanishes completely [Fig. 9(f)]. In the latter case, the circle radius is precisely equal to χ_{NR}. This discussion is actually adequate for most types of double (vibrational + electronic or electronic + electronic) resonances in gases. The line shapes are in fact more complicated as there is no reason for the product of transition moments in α_R to be real.

The discussion of absorption continua is generally difficult because we possess no closed-form expression for χ_R. However, good insight can be provided by assuming a Lorentzian distribution for the joint density of states $g(\omega_{\alpha a})$, with width Γ large compared with ω_{ba} (Fig. 10). Then, with the above assumptions ($\rho_{bb}^{(0)} \simeq 0$, ω_L fixed in resonance into the continuum), it is legitimate to still express α_R for a given Raman line

$$\alpha_R \propto (\omega_{\alpha a} - \omega_L - i\Gamma)^{-1}(\omega_{\alpha a} - \omega_a - i\Gamma)^{-1}$$

$$\simeq (\omega_{\alpha a} - \omega_L - i\Gamma)^{-2}. \quad (25)$$

As in the previous case, χ_R still describes a circle, but the rotation θ is actually doubled. This analysis provides a simple explanation for the dispersive behavior of weak resonances reported in Refs. 16 and 45, since a continuous passage from the minimum at $\theta = 90°$ to a maximum at $\theta = 270°$ [Figs. 11(a) and 11(b)] can be directly visualized (for real μ's, θ varies from 0 to 360°).

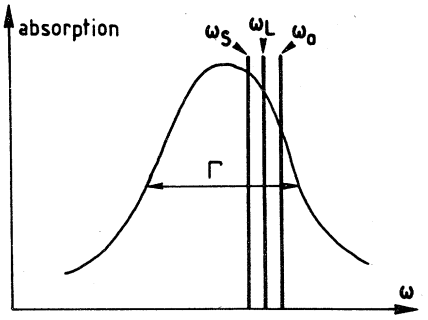

FIG. 10. Spectral configuration for CARS resonance enhancement in a continuum with a Lorentzian contour. The CARS spectrum is supposed to be of limited extent, so that $\omega_L - \omega_S \ll \Gamma$.

C. Parameter space for resonance CARS in analytical chemistry

One of the most important applications of CARS in gases is the measurement of concentrations and temperatures, using high-power-pulsed lasers.[5,9,18,47] Off resonance, the intensities of the lines are directly related to the populations of the molecular levels, so that temperatures can be determined if a Boltzmann equilibrium is established. Rotational temperatures are therefore obtained from two or more rotational lines in the same vibrational band, vibrational temperatures from two or more lines pertaining to a fundamental and a hot band[47]; alternately, Q-branch envelopes can be used if the lines are not resolved.[18] If the temperatures are known, either through a CARS spectral analysis or from conventional probe measurements, then the number density is obtained from the intensity of any of the lines. In these measurements, the major causes of error are the Raman linewidth $2\Gamma_{ba}$, which may depend slightly upon rotational quantum number and vary as a function of temperature and pressure, and the vibrational population perturbation which is caused by stimulated Raman scattering if the pump beams are too intense.[18]

If resonances with discrete absorption lines are established, these difficulties are aggravated: the intensities of the lines no longer depend solely on level populations, but also on the detunings $\omega_{na} - \omega_L$ and $\omega_{n'a} - \omega_a$, on the linewidths and the transition moments. Furthermore, the populations of the levels in resonance with the laser fields may change as a result of one-photon absorption. Concomitantly, these levels are perturbed by the optical Stark effect which causes lineshifts and broadenings.

1. Influence of selection rules on relative line intensities

Section III A was devoted to the positions of the doubly resonant features found in the CARS spectrum, and to the influence of the detunings from ω_{na}, $\omega_{n'a}$, or ω_{ba} upon their intensities, without consideration for the strengths of vibrational and rotational transition moments. Here we wish to examine how the CARS line intensity scales with the vibrational and rotational parameters. This investigation is rendered necessary by the fact that, although selection rules in off-resonance CARS are the same as in spontaneous Raman scattering,[44] resonance enhancement results in quantitative differences in the intensities (and even leads to the appearance of the double-electronic-resonance features, which are not observed in Raman scattering).

Several years ago, Barak and Yatsiv had examined the simpler problem of resonant CARS in metal vapors.[48,49] Molecular transitions introduce added complexity because of the presence of rovibrational degrees of freedom. Here we shall outline the discussion for homonuclear diatomic molecules only. The case of other molecules is more complex, but can be treated along the same guidelines. We shall also assume the three fields to be linearly polarized in the X direction (generalization to all polarization arrangements is straightforward).

Let us consider, for instance, the vibrational and rotational transitions impwed in a double resonance when ω_L is tuned in resonance with a specific transition ω_{na}. There is only one state $|n\rangle$ involved in the CARS susceptibility, but several $|n'\rangle$ and $|b\rangle$ states give contributions which interfere with one another when the summation over n' (Raman resonance) or b (double electronic resonance) in (8) is performed. Using the transformation matrix from the fixed frame (X, Y, Z) to the molecular frame (x, y, z) one has

$$\mu_{an} = \langle a|P_X|n\rangle = \langle a|P_x \cos\theta|n\rangle , \tag{26}$$

where θ is the angle between the molecular axis x and the X axis. The contribution from a particular set of levels $|n'\rangle$ and $|b\rangle$ to the susceptibility is then [we only consider the leading term $A\alpha$ in (9)]

$$\chi_R(n', b) = \frac{\rho_{aa}^{(0)}}{\omega_{ba} - \omega_L + \omega_S - i\Gamma_{ba}} \times \frac{\langle e, v_3|P_x|e', v_2\rangle\langle e', v_2|P_x|e, v_1\rangle}{\omega_{na} - \omega_L - i\Gamma_{na}} \times \frac{\langle e, v_1|P_x|e', v_4\rangle\langle e', v_4|P_x|e, v_3\rangle}{\omega_{n'a} - \omega_a - i\Gamma_{n'a}} \times S(J_1, J_2, J_3, J_4) . \tag{27}$$

Here $|e, v\rangle$ stands for the usual vibronic state in the Born-Oppenheimer approximation; e and e' are the ground and excited electronic states, respectively, and $S(J_1, J_2, J_3, J_4)$ is a rotational factor. Indices 1, 2, 3, 4 are assigned to states $|a\rangle$, $|n\rangle$, $|b\rangle$, and $|n'\rangle$, respectively. Using (26), we

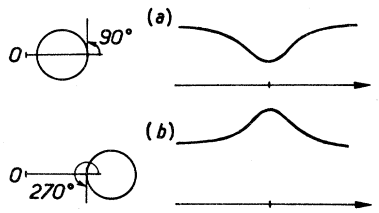

FIG. 11. Extension of the diagrams of Fig. 9 to specific situations of resonance with a continuum.

obtain

$$S(J_1,J_2,J_3,J_4) = \sum_{M_1,M_2,M_3,M_4} \langle J_3,M_3|\cos\theta|J_2,M_2\rangle \times\langle J_2,M_2|\cos\theta|J_1,M_1\rangle\langle J_1,M_1|\cos\theta|J_4,M_4\rangle \times\langle J_4,M_4|\cos\theta|J_3,M_3\rangle, \quad (28)$$

where J_i, M_i are the usual rotational quantum numbers. Operator $\cos\theta$ does not change M, so that each M contribution adds incoherently in $S(J_1,J_2,J_3,J_4)$. One then has

$$S(J_1,J_2,J_3,J_4) = \sum_M \langle J_3,M|\cos\theta|J_2,M\rangle \times\langle J_2,M|\cos\theta|J_1,M\rangle \times\langle J_1,M|\cos\theta|J_4,M\rangle \times\langle J_4,M|\cos\theta|J_3,M\rangle, \quad (29)$$

which can be easily calculated from the properties of Legendre polynomials.

As an example, let us consider the $[R,Q]$ double resonance depicted in Fig. 6(a). We have, in this instance, $v_1=v''$, $v_2=v'$, $v_3=v''+1$, $J_1=J_3=J$, $J_2=J+1$. Furthermore, rotational selection rules give only two possible values for J_4: $J_4=J\pm1$. The final susceptibility is now obtained by summing over all the possible vibrational levels v_4. Introducing the detunings $\Delta\omega(v_4,J_4)=\omega_{n'a}-\omega_a$ and assuming $\Delta\omega(v_4,J_4)\gg\Gamma_{n'a}$ and Γ_{na} independent of M, we obtain from (27)–(29)

$$\chi_R = \frac{i\rho_{aa}^{(0)}}{\omega_{ba}-\omega_L+\omega_S-i\Gamma_{ba}}|R_{ee'}|^4\frac{\langle v''+1|v'\rangle\langle v'|v''\rangle}{\Gamma_{na}} \times\left[\sum_{v_4}\sum_{J_4=J\pm1}\frac{\langle v''|v_4\rangle\langle v_4|v''+1\rangle}{\Delta\omega(v_4,J_4)}S(J,J_4)\right], \quad (30)$$

where we have written the transition moments in the Born-Oppenheimer approximation, i.e., $\langle e,v''|P_x|e',v'\rangle = R_{ee'}\langle v''|v'\rangle$; $R_{ee'}$ is the electronic transition moment and $\langle v''|v'\rangle$ is the complex Franck-Condon overlap integral (FCOI) (whose absolute value only can be determined from one-photon absorption experiments). The rotational factor $S(J,J_4)$ in (30) is calculated from (29) with $J_3=J$ and $J_2=J+1$. It is readily seen from (30) that the $[R,Q]$ line intensity depends on the modulus and also on the relative phases of the FCOI's within the brackets; this is also true for the other resonant CARS lines (vibrational as well as double electronic). As a result, it is impossible to predict the relative intensities of two distinct features in a resonant CARS spectrum without prior knowledge of these phases. Conversely, resonant CARS experiments could in principle allow one to determine the relative phase of two FCOI's.

However, the calculation of the $[R,Q]$ line intensity is simpler if there is only one vibrational state v_4 contributing to $A\alpha$, the other ones being too far off resonance. If we further assume that $\Delta\omega(v_4,J_4=J+1)\simeq\Delta\omega(v_4,J_4=J-1)$, we obtain for the susceptibility, in place of (30)

$$\chi_R = \frac{i\rho_{aa}^{(0)}}{\omega_{ba}-\omega_L+\omega_S-i\Gamma_{ba}}|R_{ee'}|^4\frac{\langle v''+1|v'\rangle\langle v'|v''\rangle}{\Gamma_{na}} \times\frac{\langle v''|v_4\rangle\langle v_4|v''+1\rangle}{\Delta\omega(v_4,J_4)}S(J), \quad (31)$$

with

$$S(J) = \sum_{J_4=J\pm1} S(J,J_4) = \sum_M \langle J,M|\cos\theta|J+1,M\rangle \times\langle J+1,M|\cos\theta|J,M\rangle\langle J,M|\cos^2\theta|J,M\rangle = \frac{J}{15}\frac{4J+1}{2J+1}. \quad (32)$$

In that case, the $[R,Q]$ line intensity depends only upon $S(J)$, $|R_{ee'}|$ and on the absolute value of the FCOI's, which are known. This is true for any resonant CARS line which receives contributions from only one Raman transition $v_1\rightarrow v_3$, one vibrational state v_2, and one vibrational state v_4; the susceptibility is then obtained by summing the two appropriate factors $S(J_1,J_2,J_3,J_4)$ in (27), resulting in a net rotational factor $S(J)$. These factors $S(J)$ are given in Table I for (a)-type Raman resonances [(c)-type resonances give identical results] and double electronic resonances. The resonance depicted in Fig. 6(a) we have labeled $[Q(v''+1-v''),R(v'-v''),p+r(v'+1-v'')]J$ where $v_4=v'+1$. The first transition listed is the Raman transition ω_{ba}, the second and third ones are the ω_{na} and $\omega_{n'a}$ transitions, respectively. Upper-case lettering is used

TABLE I. Rotational factors of the double resonances, grouped according to their expressions.

$[\omega_{ba},\omega_{na},\omega_{n'a}]\ J'$	$[Q,R,(p+r)]\ J-1$ $[(q+o),P,P]\ J$	$[Q,P,(p+r)]\ J$ $[(q+s),R,R]\ J-1$	$[O,P,p]\ J;[q,P,R]\ J$ $[S,R,r]\ J;[q,R,P]\ J$
$S(J')$	$\frac{J}{15}\frac{4J+1}{2J+1}$	$\frac{J}{15}\frac{4J-1}{2J-1}$	$\frac{J}{15}\frac{2J+2}{2J+1}$

for the transitions which are in exact or near exact resonance with the field frequencies, lowercase lettering otherwise. For the latter, depending on rotational selection rules, one or two transitions are possible and listed accordingly. Under certain experimental conditions, one of these two allowed transitions is also in near resonance (triple resonance), so that the contribution of the other one is then negligible. This situation was encountered experimentally in the resonant CARS spectrum of iodine, which is discussed below in Sec. V. In that case the rotational factor is made up of the one relevant factor $S(J_1, J_2, J_3, J_4)$ in (27). We have not listed these in the table because their expression is not as simple as that of $S(J)$. In Table I the vibrational quantum number is omitted since we are only interested in the rotational part of the transition moments.

As in RS,[42] the relative intensities of the successive overtones of a given Raman line change drastically when going from off resonance to on resonance. In off-resonance CARS (as in RS), the ratio of intensities of the nth overtone to the fundamental is rapidly decreasing with n since it scales as

$$\left| \sum_{q+p=n} \frac{\partial^p}{\partial Q^p} R_{ee'} \frac{\partial^q}{\partial Q^q} R_{ee'} \langle v'' | Q^n | v'' + n \rangle \right|^2 \times \left(\left| R_{ee'} \frac{\partial}{\partial Q} R_{ee'} \langle v'' | Q | v'' + 1 \rangle \right|^2 \right)^{-1},$$

where Q is the usual vibrational coordinate. On resonance, on the contrary, the intensities of the successive overtones depend only on the phases and magnitudes of the FCOI's and vary erratically.[42]

2. Collisional broadening

Elastic and inelastic collisions are, under usual conditions and for an excitation resonant with discrete absorption lines, the main broadening mechanisms contributing to Γ_{na}, Γ_{nb}, $\Gamma_{n'a}$, $\Gamma_{n'b}$, Γ_{ba}, and $\Gamma_{nn'}$ appearing in Eqs. (8) and (10). As a matter of fact, since the dominant spectral characteristics are obtained from terms $A\alpha$ and $C\gamma$ in (9), only Γ_{na}, $\Gamma_{n'a}$, Γ_{nb}, and Γ_{ba} need to be considered. In the following, we assume, as in Sec. III A, that ω_L is held fixed. In the off-resonance case ($|\omega_{na} - \omega_L| \gg \Gamma_{na}$), Γ_{na} and Γ_{nb} then have little influence on the CARS spectrum and do not have to be measured. The intensity and width of a vibrational resonance depend only on Γ_{ba}, those of an electronic resonance only on $\Gamma_{n'a}$; both Γ_{ba} and $\Gamma_{n'a}$ are easily retrieved from the spectral contour if the lines are resolved. If strict or near resonance is achieved on ω_L, then Γ_{na} and Γ_{nb} must be determined by an independent measurement (only Γ_{na} must be measured if $\rho_{bb}^{(0)} = 0$). For media with stable composition, pressure and temperature, these measurements need not be carried out simultaneously. In unstable media, however, simultaneity is necessary, which may render the experiments extremely delicate to perform. In this case, the spectra will be best recorded using a multiplex CARS setup[7]; Γ_{ba} and $\Gamma_{n'a}$ can in principle be derived from such spectra, but not Γ_{na} nor Γ_{nb}. If elastic collisions dominate, all the Γ's are nearly equal, so that the analysis is facilitated. Resonance enhancement from a dissociative continuum is, in these respects, much easier to investigate since all the Raman resonances are equally enhanced in practice and since the complication resulting from the Γ_{na}'s is eliminated.

3. Population perturbation

We have discussed in Sec. II B 2 and in Appendix B some of the changes in vibrational populations that occur during CARS measurements. Changes are actually caused both by CARS and by stimulated Raman scattering (which takes place along with CARS). Off resonance, the latter dominates.[18,19] On resonance, all the rotational-vibrational perturbations are strongly enhanced; in addition, saturation of the one-photon transitions also takes place and may become the cause of a comparable and even larger perturbation. Unless all these perturbations can be accurately determined, they must be avoided as they bias the measurements and distort the spectra.

To proceed, a picture of the various molecular relaxation mechanisms must be established. Unfortunately, no universal model can be presented. Relaxation rates vary extremely widely from one species to the other and depend strongly upon thermodynamic variables. Elastic collisions may or may not dominate the line-broadening mechanism. Moreover, rotational relaxation within a vibrational state is usually orders of magnitude faster than relaxation between adjacent vibrational states in the ground electronic state, and these rates are themselves radically different in the excited electronic state. The simplest approach is of course to assume that a single rate (Γ_{bb}) is sufficient to describe these processes in the ground electronic state (and similarly in the excited state).

The population perturbations can be represented as higher-order corrections to the initial populations $\rho_{aa}^{(0)}$ and $\rho_{bb}^{(0)}$ in the expression of $\chi^{(3)}$. Second-order corrections $\rho_{aa}^{(2)}$, $\rho_{bb}^{(2)}$, $\rho_{nn}^{(2)}$, and $\rho_{n'n'}^{(2)}$ apply for one-photon absorption. For instance, we have for $\omega_{na} \simeq \omega_L$

$$\frac{\partial}{\partial t}(\rho_{nn}^{(2)}-\rho_{aa}^{(2)})=\frac{4\rho_{aa}^{(0)}}{\hbar^2}\frac{\Gamma_{na}|\mu_{na}|^2|E_L|^2}{(\omega_{na}-\omega_L)^2+\Gamma_{na}^2}-\Gamma_{nn}\rho_{nn}^{(2)}+\Gamma_{aa}\rho_{aa}^{(2)}. \tag{33}$$

Saturation by stimulated Raman scattering is reflected in corrections of the form $\rho_{aa}^{(4)}$ and $\rho_{bb}^{(4)}$. These corrections can be calculated readily by means of time-ordered diagrams; they are similar to, and much larger than, those for CARS, which are derived in Appendix B. On resonance, the main corrective term is, assuming $\rho_{bb}^{(0)}=0$

$$\frac{\partial}{\partial t}(\rho_{bb}^{(4)}-\rho_{aa}^{(4)})=\frac{\rho_{aa}^{(0)}}{\hbar^4}|E_L|^2|E_S|^2\left\{2\,\mathrm{Im}\left[\frac{\mu_{bn}\mu_{na}}{\omega_{ba}-\omega_L+\omega_S+i\Gamma_{ba}}\frac{\mu_{an}\mu_{nb}}{\omega_{na}-\omega_L+i\Gamma_{na}}\left(\frac{1}{\omega_{na}-\omega_L+i\Gamma_{na}}+\frac{1}{\omega_{nb}-\omega_2-i\Gamma_{nb}}\right)\right]\right.$$
$$\left.-\left(\frac{\Gamma_{na}\Gamma_{nb}}{4\Gamma_{nn}}\right)\frac{\mu_{bn}\mu_{na}}{(\omega_{nb}-\omega_S)^2+\Gamma_{nb}^2}\frac{\mu_{an}\mu_{nb}}{(\omega_{na}-\omega_L)^2+\Gamma_{na}^2}\right\}-\Gamma_{bb}\rho_{bb}^{(4)}+\Gamma_{aa}\rho_{aa}^{(4)}. \tag{34}$$

The first term between brackets is the usual Raman term, whereas the second one corresponds to the hot luminescence part of the scattering. If we ignore elastic collisions ($\Gamma^e=0$), assume that the resonant gas is diluted in a buffer gas at STP, and take realistic values for Γ and $|\mu|$ [$\Gamma/2\pi c=0.2$ cm^{-1},[49] $|\mu_{na}|=0.1D$ (Ref. 50)] we arrive at a maximum steady-state power density $I_L=10$ MW/cm^2 for one-photon saturation [$I_L=(c/2\pi)E_L^2$]. For this value, the population difference from (33) is $0.45\rho_{aa}^{(0)}$ on resonance (for such a high level of perturbation, higher-order corrections are actually necessary). If I_L is kept just below the one-photon saturation level, Raman saturation will begin for about the same level in I_S, corresponding to power densities $I_S=10$–50 MW/cm^2 (if $|\mu_{bn}|=|\mu_{na}|$).

If elastic collisions are also taken into account, then larger values of I_L and I_S are needed to cause saturation. If the disparity between rotational and vibrational relaxation in the ground electronic state is important, the model can be refined to some extent[27] by distinguishing between the rotational rates Γ_{aa}^r and Γ_{bb}^r, representing population relaxation within each vibrational state, and the vibrational rates Γ_{aa}^v and Γ_{bb}^v, representing the relaxation of the total population of the rotational manifold into neighboring vibrational levels. Typically, $2\pi(\Gamma^r)^{-1}<10^{-9}$ s, $2\pi(\Gamma^v)^{-1}<1$ μs at STP. Then, depending on the pulse duration τ_p, three regimes can be recognized: (i) $2\pi(\Gamma_{aa}^r)^{-1}<\tau_p<2\pi(\Gamma_{aa}^v)^{-1}$, the regime that usually prevails in pulsed CARS work ($\tau_p\simeq 10ns$), and for which the above estimates of power densities were obtained ($\Gamma_{aa}=\Gamma_{aa}^r$; $\Gamma_{bb}=\Gamma_{bb}^r$); (ii) $\tau_p<2\pi(\Gamma_{aa}^r)^{-1}$, the fully transient regime, for which relaxation during the pulse is unimportant and higher power densities can actually be tolerated; (iii) $\tau_p>2\pi(\Gamma_{aa}^v)^{-1}$, the true steady-state regime, for which the estimate obtained from (33) remains valid, but that from (34) must be corrected using $\Gamma_{aa}=\Gamma_{aa}^v$ and $\Gamma_{bb}=\Gamma_{bb}^v$, thus giving a much lower ceiling on I_S.

4. *Optical Stark effect*

When ω_L is near resonance ($\omega_L\simeq\omega_{na}$), and if the power density is high, new equilibrium populations are established in $|a\rangle$ and $|n\rangle$ as discussed in Sec. III C 3. Simultaneously new spectral components are found in the resonances of the molecular system (optical Stark effect). For very high densities, the resonant coupling between field and molecules must be treated to all orders of perturbation.

The optical Stark effect in three-level systems has been studied recently, both in RF and RRS as well as in resonant two-photon absorption.[51-59] Although the molecular system has at least four levels in interaction with the fields in resonant CARS, we can assume it to be a three-level system $|a\rangle$ $|n\rangle$, $|b\rangle$ (with no elastic collisions) for the purpose of a semiquantitative spectral analysis of the vibrational features (double resonance on ω_{na} and ω_{ba}, with $\omega_{n'a}\neq\omega_a$). We then expect a splitting of the Raman resonance into two components. The splitting depends upon the power density and the detuning. Numerous situations can be found depending on the relative magnitudes of the Rabi frequency, of the detuning, and of Γ_{nn}. For the sake of simplicity, we will only discuss two representative cases.

Near resonance ($|\omega_{na}-\omega_L|>\Gamma_{nn}$, $2|\mu_{na}||E_L|/\hbar$), the coupling between field and molecules is weak enough to allow a diagrammatic perturbative approach. We then expect the polarization at ω_a to contain in addition to the usual third-order term possessing a resonance at $\omega_L-\omega_S=\omega_{ba}$, a fifth-order term giving a much weaker resonance at $\omega_L-\omega_S=\omega_L-\omega_{nb}$. The latter, however, becomes large near saturation. It can be calculated by adding two interactions at ω_L on the diagrams of Figs. 1–3 and retaining the time-orderings that give the largest contributions.

On resonance ($|\omega_{na}-\omega_L|<\Gamma_{nn}$), the two components are found at $\omega_L-\omega_S=\omega_{ba}\pm\Omega$ with $\Omega=2|\mu_{na}||E_L|/\hbar$ and are of comparable intensities. This result is obtained assuming that the laser field saturates the ω_{na} transition ($\Omega>\Gamma_{nn}$) whereas the Stokes field is weak and nonsaturating. Since μ_{na} depends on the absolute value of the rotational

quantum number M for P or R transitions, each component $\pm M$ of the ω_{na} transition undergoes a distinct splitting. This effect could in principle be seen in CARS with high-resolution cw sources. However, applications in analytical chemistry require use of pulsed lasers, so that an additional broadening of the split components will take place due to temporal as well as spatial nonuniformity of the laser power density in the focal region. Therefore, the M components are unlikely to be resolved.

The amount of splitting (or broadening) under practical experimental conditions is easily estimated. Using, as in Sec. III C 3, $|\mu_{na}| = 0.1D$ and a power density of 10 MW/cm^2, we arrive at $\Omega/2\pi c \simeq 0.1$ cm^{-1}, which is comparable to the linewidth (0.2 cm^{-1}), and is thus the cause of an appreciable spectral distortion.

Concerning double electronic resonances, analogous splittings are anticipated as ω_a is swept across the $\omega_{n'a}$ resonances. The three-level system under consideration here is then composed of $|a\rangle$, $|n\rangle$ and $|n'\rangle$, ω_{na} being the resonant transition under saturation.

This analysis should be refined by considering all four levels interacting with the fields ($|a\rangle$, $|n\rangle$, $|b\rangle$ and $|n'\rangle$), by allowing for elastic collisions and taking a more accurate model for collisional and radiative damping.

5. *Resonant CARS in analytical chemistry*

Off resonance, CARS has already been shown to be a superior tool for the Raman spectroscopy of gases. Resonance enhancement adds a new dimension to this technique and considerably extends the potential of CARS: both resonant Raman scattering and one-photon spectroscopy can be handled in an elegant manner, as was discussed in Sec. III A. The impact in analytical chemistry is expected to be just as important. In conventional CARS, the detectivity is limited by χ_{NR} interference at mixing ratios of 10^{-3}–10^{-5}.[18,19] Resonance enhancement can improve this performance significantly.

The improvement can be estimated readily, using experimental results on the scattering cross section ($d\sigma/d\Omega$) in RRS. Assuming $\rho_{bb}^{(0)} = 0$ and $\omega_L \simeq \omega_{na}$, one has

$$\chi_R \propto \frac{\mu_{bn}\mu_{na}}{(\omega_{ba} - \omega_L + \omega_S - i\Gamma_{ba})(\omega_{na} - \omega_L - i\Gamma_{na})} \times \sum_{n'} \frac{\mu_{an'}\mu_{n'b}}{\omega_{n'a} - \omega_a - i\Gamma_{n'a}}, \tag{35}$$

and

$$\frac{d\sigma}{d\Omega} \propto \left| \frac{\mu_{bn}\mu_{na}}{\omega_{na} - \omega_L - i\Gamma_{na}} \right|^2 . \tag{36}$$

It is seen readily that χ_R scales as $(d\sigma/d\Omega)^{1/2}$ as $\omega_L \to \omega_{na}$. Using experimental data on halogen gases,[60] we thus expect gains of two or three orders of magnitude for χ_R, and equivalent improvements for the detectivity. In fact, the circle model which was discussed in Sec. III B shows that minor modifications must be made on the theory of Ref. 18 for the lowest concentrations due to the different line shapes [in particular, detection is impossible for the situation of Fig. 9(f)]. We thus expect the detectivity to be improved down into the ppm range for typical diatomic gases in mixtures at STP. This statement is supported by the experimental results reported in Sec. V. On the other hand, when the resonance is in a dissociative continuum, the three field frequencies are simultaneously resonant. Then, the enhancement is the same as for $d\sigma/d\Omega$, i.e., one to three orders of magnitude.[61] Instrumentally, limitations are imposed by dispersion and by one-photon attenuation of the light waves, as well as by population perturbation and the concomitant Stark broadening.

Using $E(z,t) = E\exp(-i\omega t + ikz) + \text{c.c.}$, with $k = \sqrt{\epsilon}\,\omega/c$, $\epsilon = 1 + 4\pi\chi^{(1)}(\omega)$, we see that attenuation is given by $I_L(z) = I_L(0)\exp(-\alpha_L z)$, with $\alpha_L \simeq 4\pi(\omega_L/c)\,\mathrm{Im}[\chi^{(1)}(\omega_L)]$ at frequency ω_L if the medium is homogeneous. Similar equations hold at ω_S and ω_a. Assuming ω_L is near a resonance and neglecting the buffer gas contribution,[28,35] we have

$$\chi^{(1)}(\omega_L) \simeq N\rho_{aa}^{(0)} |\mu_{an}|^2/\hbar(\omega_{na} - \omega_L - i\Gamma_{na}). \tag{37}$$

Taking $|\mu| = 0.1D$, $\Gamma/\pi c \simeq 0.4$ cm^{-1}, $\rho_{aa}^{(0)} = 10^{-2}$ and $N = 3.10^{16}$ cm^{-3} (1000 ppm at STP), we find $\alpha_L = 0.1$ cm^{-1} in the visible on resonance. If $\alpha_L = \alpha_S = \alpha_a$, the sample being contained in a 2-cm-long cell and the beams focused in the center, the anti-Stokes power is reduced by 30% with respect to a transparent sample situation. This attenuation is independent of the total gas pressure p, since N and Γ are proportional to p (this is not true for an absorption continuum).

Dispersion (phase matching) is governed by $\mathrm{Re}(\chi^{(1)})$. One can easily demonstrate that the coherence length remains large compared to typical beam confocal parameters for the above experimental conditions; no reduction in signal is thus anticipated.[27]

For large concentrations, attenuation and phase mismatch become prohibitive. However, off-resonance measurements then become easy, eliminating the need for resonance enhancement. For smaller concentrations (down to those for which $|\chi_R| = \chi_{NR}$), the sole problems that remain are those of population perturbations and Stark broadening. Given pulse duration τ_p, $\chi^{(3)}$, number

of photons to be collected (hence given $P_L^2 P_S$) and saturation densities I_L, I_S, the central question is that of the limiting F number for the optics. This problem was discussed in Ref. 18 for the off-resonance case. We know (see Sec. V) that double resonances can be found in I_2 such that the CARS susceptibility is 4.10^2 times larger than in usual nonresonant gases (like O_2, N_2, etc.) under the same thermodynamic conditions. Using (1), we arrive at the conclusion that powers on the order of 3 kW are necessary to collect 10^4 photons in 1 μs from 10-ppm I_2 in air, with $|\chi^{(3)}| = 4.10^{-18}$ cm^3/erg. Power densities for saturation and Stark broadening are typically 10 MW/cm^2 under those conditions. In fact, one can tolerate about ten times as much at the focus due to temporal and spatial nonuniformities, so that the F number should be on the order of 100 or more. The longitudinal spatial resolution, which is on the order of a few times the confocal parameter, is thus about 1 cm.

IV. TRANSIENTS IN CARS AND FLUORESCENCE INTERFERENCE

The coherency of the CARS signal and its position to the anti-Stokes side of the pump allow good discrimination against interfering spontaneous emissions such as chemiluminescence and laser-induced fluorescence. However, radiative de-excitation of the probed molecules raised into intermediate states by one-photon absorption may compete and interfere with the anti-Stokes generation. The influence of these phenomena on CARS may be apparent, for instance, during the transient build up and decay under pulsed excitation.

The transient behavior of CARS is expected to be quite different from that of RRS, for which fluorescence interference is a major drawback. This is important since it may shed light on the recent controversies concerning the distinction between the incoherent spontaneous two-step fluorescence emission (also interpreted as hot luminescence or redistribution emission) and the one-step Raman emission in RRS.[23,26,42,62-65] We shall here review some of the transient results in RRS, and then discuss the behavior of the most characteristic RVR and NVR terms in CARS by means of the diagrammatic representation. This analysis of transient CARS is related to the recent studies of transients in nonlinear optic such as Ramsey fringes, photon echo and free induction decay by Shen,[66] Salour, Brewer *et al.*, Cagnac *et al.*, Liao *et al.*, and Loy,[67] and also to picosecond studies of broadening effects of Raman lines.[17]

In RRS it is difficult to establish a precise distinction between fluorescence and Raman scattering, since both are spontaneous processes with overlapping spectra. It is nonetheless important to either isolate one from the other or provide a correct interpretation of the total response in order to retrieve meaningful data from the Raman spectrum. For this reason, there have been many experimental[42,62,65,68] and theoretical[23,42,64,69,70] investigations on RRS and fluorescence. The question has been raised as to whether these are the same physical process or two distinct and almost simultaneous processes. Shen,[23] in particular, has interpreted RRS as composed of both a Raman and a hot luminescence components that have different spectral contents and temporal behaviors. He used the density matrix approach to calculate the nonlinear polarization at frequency ω_S, $\vec{P}^{(3)}_{NL}(\omega_S, t)$, which is shown to consist of two components: (i) one arises from the nondiagonal density matrix term $\rho^{(2)}_{ba}(\omega_L - \omega_S, t)$ and is identified as Raman scattering, since it represents an excitation of the vibrational mode of frequency ω_{bq}; (ii) the other comes from the diagonal terms $\rho^{(2)}_{nn}(0,t)$ and is characterized as hot luminescence since $N\rho^{(2)}_{nn}(0,t)$ is the population brought into state $|n\rangle$ by one-photon absorption. It is precisely the part of $N\rho^{(2)}_{nn}(0,t)$ which is proportional to Γ^e that gives the redistribution radiation of Ref. 42. Hot luminescence is usually small, but becomes as important as the Raman component when the pump frequency comes close to an electronic resonance. When there is only one excited state $|n\rangle$ involved in the scattering, the damping of component (ii) after the laser excitation is turned off is, *a priori*, slower than that of component (i) since its decay time is Γ_{nn}^{-1} as compared to Γ_{na}^{-1}; however this is not always the case, especially for gases with closely spaced levels. It has been shown recently by Brewer *et al.*[67] that, for the transition $R59$ (15–2) of the electronic transition $^3\Pi^+_{ou} - {}^1\Sigma^+_g$ of I_2, the inelastic and elastic collision cross sections are of the same order of magnitude, respectively, 530 and 780 Å^2. Unfortunately, combustion gases and reactive media present absorption lines which are broad and closely spaced, so that there are several near-resonant neighboring states $|n\rangle$ coupled to one another through several distinct relaxation mechanisms: radiative and elastic collisional damping, rotational and vibrational transfers by inelastic collisions. The equations of motion (2) for the $\rho^{(2)}_{nn}(0,t)$'s are then coupled to each other through these damping terms [see Eq. (3)], and the calculation of transients is, then, rather cumbersome.

The separation of transient RRS into hot luminescence and Raman scattering has also been discussed by means of the diagrammatic repre-

sentation.[22] One can describe $\vec{P}^{(3)}_{NL}(\omega_S, t)$, as was done for $\vec{P}^{(3)}_{NL}(\omega_a, t)$, by means of eight fundamental time-ordered diagrams. These can be easily drawn from the diagrams of Fig. 1 with the following modifications: (i) vertex 3 is replaced by an absorption at ω_L whenever it is an emission, and vice versa, (ii) absorption (emission) at ω_a is replaced by emission (absorption) at ω_S, (iii) each diagram must be reflected with respect to the time axis in order to depict the part of $\vec{P}_{NL}(\omega_S, t)$ oscillating as $\exp(-i\omega_S t)$ (one otherwise obtains its complex conjugate). Both parametric and nonparametric diagrams give contributions to $\vec{P}_{NL}(\omega_S, t)$; this was not correctly asserted in Ref. 22. However the parametric diagrams are one-photon antiresonant, so that their contributions are negligible in RRS. It is then apparent, from the three time-ordered possibilities for vertex 3 in the nonparametric diagrams, that the diagram derived from Fig. 1(b) provides Shen's Raman component whereas the other two describe hot luminescence.

For resonant CARS, in addition to the definition of the distinct transient components, there is the added question of their spatial coherency. The contribution of the probed molecules to $\vec{P}^{(3)}_{NL}(\omega_a, t)$ is easily derived, either directly from the time-ordered diagrams[21] or from the iterative solutions of (2). As in RRS, it can be separated quite generally into two parts: (a) an RVR component calculated from $\rho^{(2)}_{ba}(\omega_L - \omega_S, t)$ and depicted in Figs. 1(a), 1(b), and 2 which is analogous to the above Raman component (i) and provides contribution χ^{ba}_R in the stationary case; (b) an NVR component calculated from $\rho^{(2)}_{nn}(2\omega_L, t)$, and $\rho^{(2)}_{nn}(\omega_L - \omega_S, t)$ which is depicted in Fig. 3 and corresponds to the hot luminescence component (ii). Under stationary conditions, the latter gives precisely the small NVR terms in χ_{NR} which can shift some of the electronic resonances in χ^{ba}_R as discussed in Sec. II B 3. In contrast to RRS, this NVR transient remains small compared to the RVR one if $\rho^{(0)}_{bb} \simeq 0$, even in the vicinity of single photon resonances (this is the reason why there is no redistribution component in resonant CARS spectra). We shall also assume that the power density is low, so that the transients arising from $\rho^{(2)}_{nn}(0, t)$ (which result in Stark splitting of the CARS resonances in the steady state) are negligible.

We shall thus consider here the RVR transients associated with Figs. 1(a) and 2(a) which correspond to the main stationary terms $A\alpha$ and $C\gamma$ of χ^{ba}_R in (9). The pump fields are assumed to be switched on at $t = 0$ and off at $t = T$, viz.,

$$\vec{E}_{L,S}(z, t) = \hat{e} E_{L,S}(z, t) \exp(-i\omega_{L,S} t + i k_{L,S} z) \times \mathcal{U}(t)[1 - \mathcal{U}(t - T)], \tag{38}$$

where $\mathcal{U}(t)$ is the unit-step function. Upon carrying out the time integrations for the specific diagrams, one obtains

$$\begin{aligned} P^{(3)}_{NL}(\omega_a, t) = \hat{e} \circ \vec{P}^{(3)}_{NL}(\omega_a, t) = \hbar^{-3} (E^2_L(z, k) E^*_S(z, t) \mathcal{U}(t)[1 - \mathcal{U}(t - T)] \{ & \rho^{(0)}_{aa} K_1 \exp[-i(\omega_{na} + \omega_L - \omega_S - i\Gamma_{na})t] \\ & + \rho^{(0)}_{bb} K_2 \exp(-i(\omega_{bn} + 2\omega_L - i\Gamma_{bn})t) + K_3 \exp(-i(\omega_{ba} + \omega_L - i\Gamma_{ba})t) + K_4 \exp(-i\omega_a t) \\ & - (\rho^{(0)}_{aa} K_1 + \rho^{(0)}_{bb} K_2 + K_3 + K_4) \exp(-i\omega_{n'a} - \Gamma_{n'a})t \} + E^2_L(z, T) E^*_S(z, T) \mathcal{U}(t - T) \\ & \{ \}_{t=T} \exp(-i\omega_{n'a} - \Gamma_{n'a})(t - T)). \end{aligned} \tag{39}$$

Each coefficient K is a sum of terms proportional to four transition moments and three energy denominators exhibiting one- and two-photon resonances (or antiresonances); $\{ \}_{t=T}$ stands for the value of the terms between brackets for $t = T$. We conclude from (39) that (i) while the excitation is on, there are five distinct temporal contributions to $P^{(3)}_{NL}(\omega_a, t)$. (a) The first two, which contain K_1 and K_2, result from the natural response of the molecules to the first perturbation, [depicted by vertex 1 in Fig. 1(a) (2(a))] at frequency ω_{na} (ω_{bn}) with decay rate Γ_{na}(Γ_{bn}), driven by the next two interactions with the fields at $\omega_L(\omega_L)$ and $\omega_S(\omega_L)$. (b) The third one is the result of the natural response after two perturbations [depicted by vertices 1 and 2 in Figs. 1(a) and 2(a)] oscillating at ω_{ba} with damping Γ_{ba}, and driven by the last field interaction at ω_L. (c) The fourth one is the stationary solution driven at frequency ω_a. (d) The initiation of the excitation results in a natural response at $\omega_{n'a}$ with damping $\Gamma_{n'a}$ given by the fifth term. (ii) After the sudden termination of the excitation, there is only a natural response at $\omega_{n'a}$ with decay rate $\Gamma_{n'a}$ [terms proportional to $\mathcal{U}(t - T)$ in (39)] and no driven solution, contrary to the case of spontaneous RRS, because CARS is a coherent process. (iii) In addition, expression (39) contains only nondiagonal damping coefficients, i.e., those containing the collisional broadening Γ^e. If $\Gamma_{na} > \Gamma_{nn}$, the transient component of $P^{(3)}_{NL}(\omega_a, t)$ is damped faster than that of the hot luminescence part of $P^{(3)}_{NL}(\omega_S, t)$. Under usual experimental conditions, damping takes place in a time shorter than the pump pulse duration, so that interpretation of CARS experiments in terms of the CARS susceptibility given

in (8) is justified. (iv) However, in experimental situations where the Stark effect is strong and where the transient behavior of the small NVR components needs to be considered, the calculation is as cumbersome as for the hot luminescence component of RRS.

V. EXPERIMENTAL RESULTS IN I_2 AT 1 mb.

Iodine is a good candidate for an experimental verification of the properties of resonant CARS. This is because it possesses strong and sharp absorption lines throughout the visible range so that efficient laser dyes can be used, and because most of the characteristic absorption features have now been assigned.[71,72]

Our first I_2 CARS spectra were presented recently[73] and have now been interpreted.[74] We here wish to discuss this interpretation as an illustration of the theory exposed in the preceding chapters.

Specially developed flash-lamp-pumped dye lasers are used in this experiment. Their characteristics are the following: (i) pulse duration 1 μs, (ii) peak power up to 10 kW, (iii) beam divergence less than 1.5 times the diffraction limit, (iv) line-width 0.15 cm^{-1} or less, and (v) beam diameter 2.2 mm. Special attention was paid to dye solvent temperature regulation and alignment stability. The spectra, in this preliminary work, were recorded without the help of a reference; this has probably caused an artificial broadening of the lines, and possibly some distortion from one end of the spectra to the other, since dye aging and possible slight beam wandering were not compensated for. Other instrumental details on the CARS setup will be found in Ref. 74. Focusing of the beams into the I_2 sample was performed by means of a 12-cm focal length lens. The I_2 was contained in a temperature-controled cell to vary the partial pressure; air at 1 atm was used as a buffer gas. The spectra reported herein were obtained at 35 °C, corresponding to 1 mb of I_2.[75] The cell length used for these experiments was 10 cm. This value is a compromise between the need to avoid generation of a nonresonant signal by cell windows and the need to minimize attenuation by I_2 at all wave-lengths.

The exciting light was in a spectral region easily covered by Rhodamines 6 G and 640 and for which the I_2 absorption lines are identified. The vicinity of the Na D line at 16 956.18 cm^{-1} was selected for ω_L. The latter was tuned as close as possible to that line, with a precision estimated at ±0.5 cm^{-1}. Two different techniques were used to evaluate beam attenuation. We compared the

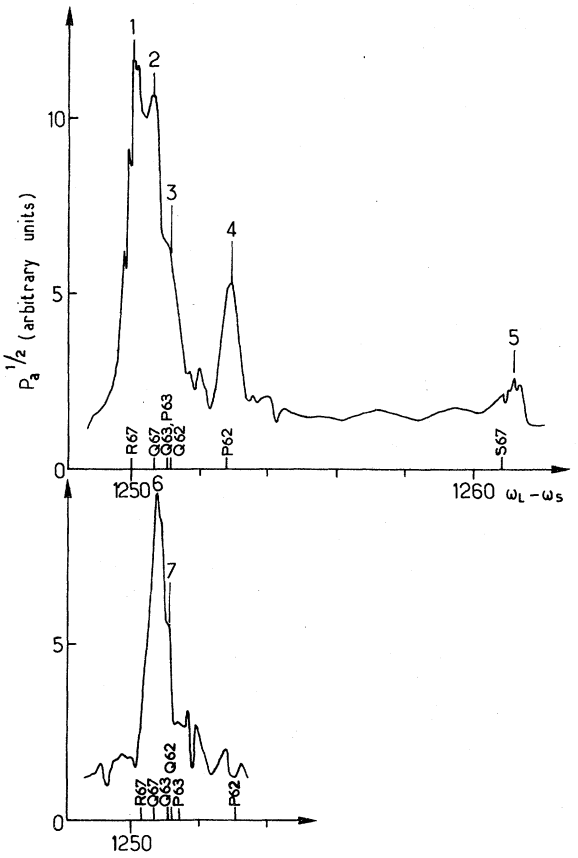

Fig. 12. CARS spectra of I_2 in air at 35 °C (partial pressure 1 mb), for ω_L tuned in a region about 16 956 cm^{-1} (a), then downshifted by 0.3 cm^{-1} (b). No reference cell was used, so that amplitude distortions may be present especially between (a) and (b). The positions of the strongest double resonances are also indicated.

(off-resonance) CARS spectrum of the O_2 present in the cell with that of O_2 in room air (see Fig. 11). The latter was twice as strong, which gives an average attenuation of 20% for the full cell length at ω_L, ω_S, and ω_a after correction for window losses. This result was verified by placing the cell before and after the focus and monitoring the resultant reductions in the CARS signal. These experiments establish that little spectral distortion will take place and that phase matching is not impaired.

The driving mechanism that tunes ω_S was then calibrated relative to ω_L by recording the CARS spectrum of the four sharp resonances of the CO_2 molecule (ν_1, ν_1', $2\nu_2$, $2\nu_2'$) which lie precisely in the region of interest. The accuracy of this calibration is about 0.1 cm^{-1}. Then we scanned most of the fifth vibrational overtone of I_2 about (1261 cm^{-1}) [Fig. 12(a)]. When ω_L was downshifted by 0.3 cm^{-1}, Fig. 12(b) was obtained. The resonances in these spectra are very strong, about twice as

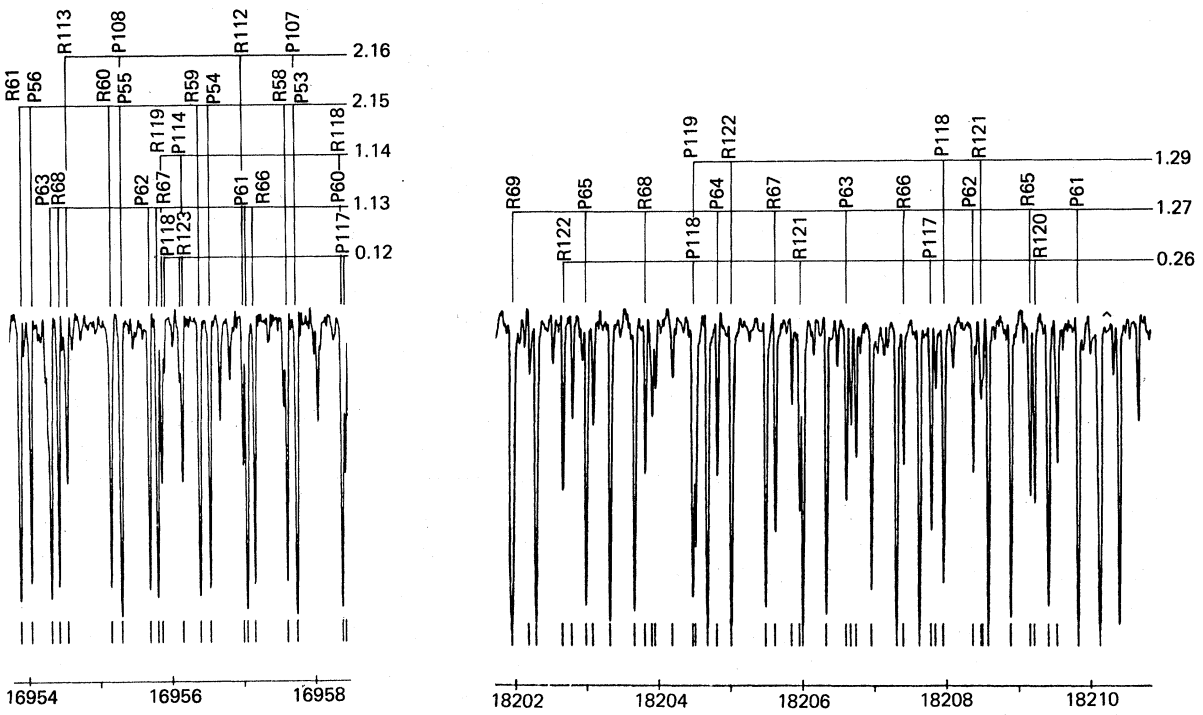

FIG. 13. Absorption spectrum of pure I_2 at room temperature and 0.4 mb. Only the regions of interest for ω_L and ω_a are given. Horizontal scale is in cm^{-1} (after Ref. 76).

intense as the peak of the Q branch of the O_2 contained in the cell (and whose partial pressure is about 180 mb).

Assignment of the most conspicuous features in Fig. 12 can be done using the high-resolution absorption spectrum of I_2 obtained by Gerstenkorn and Luc[76] (Fig. 13). Table II lists the most probable double resonances responsible for them, given the uncertainties in ω_L and ω_S, and the smearing of the lines due to collisional broadening by air. Three rotational sublevels of the $v''=1$ state have been found to give large potential contributions. These levels are $J=62, 63, 67$. We assumed $\omega_L = 16\,995.6\ cm^{-1}$, which is the most probable value as is justified *a posteriori* by the analysis. The strongest features, which are labeled 1 and 2, correspond to $J=67$ and benefit from enhancement by the $R67$ (13 – 1) one-photon

TABLE II. I_2 absorption lines and resonances used for assignment of our CARS spectra, with corresponding detunings $\omega_{na} - \omega_L$. The Raman resonances in the spectrum are found at $\omega_L - \omega_s = \omega_{ba}$, the double electronic ones at $\omega_L - \omega_s = \omega_{n'a} - \omega_i$.[a]

$\lvert a > J$ number	ω_{ba}[b]	ω_{na}	$\omega_{n'a}$	$\omega_L = 16\,955.6$		$\omega_L = 16\,955.3$	
				$\omega_{na} - \omega_L$	$\omega_{n'a} - \omega_L$	$\omega_{na} - \omega_L$	$\omega_{n'a} - \omega_L$
62	Q 62 (7-1) 1251.15	P 62 (13-1) 16 955.7	P 62 (27-1) 18 208.4	0.1	1252.8	0.4	1253.1
63	Q 63 (7-1) 1251.07	P 63 (13-1) 16 954.3	P 63 (27-1) 18 206.6	-1.3	1251.0	-1.0	1251.3
67	Q 67 (7-1) 1250.72	R 67 (13-1) 16 955.8	R 67 (27-1) 18 205.6	0.2	1250.0	0.5	1250.3

[a] All ω values given in cm^{-1}.

[b] Calculated from the spectroscopic constants of Ref. 77.

absorption in the vicinity of ω_L. Feature 1 probably gets its strongest contribution from the double electronic resonance, which corresponds to ω_a sweeping the $R67\ (27-1)$ absorption, and is therefore found at $\omega_L - \omega_S = \omega_{n'a} - \omega_L = 1\,250.0$ cm^{-1}. For this particular double electronic resonance, the possible $|b\rangle$ levels in the scheme of Fig. 6(b) are found from selection rules to be $v=7$, $J=67$ and 69. The strongest contribution comes from $v=7, J=67$, which corresponds to the $Q67(7-1)$ fifth overtone Raman resonance. We shall therefore label this resonance $[q(7-1), R(13-1), R(27-1)]\,67$ in the notation of of Sec. III C 1. Feature 2 coincides with a Q line, which we write $[Q(7-1), R(13-1), r(27-1)]67$. Since features 1 and 2 correspond to the same $|a\rangle$ and $|b\rangle$ states and are very close, they strongly enhance one another (this case is almost a triple resonance as discussed in (d) of Sec. III A 1). Feature 2 furthermore receives a small contribution, which is of the $[Q,R,p]$ type, from the $P67(27-1)$ absorption line lying at 18 199.26 cm^{-1}. The latter also produces a weak $[q,R,P]67$ double electronic resonance at 1 243.5 cm^{-1}, outside the spectral range of Fig. 12. This line constitutes a doublet in association with $[q,R,R]67$, as discussed in (b) of Sec. III A 1. Finally, the Raman resonance $S67(7-1)$ produces a CARS line $[S(7-1), R(13-1), r(27-1)]67$ at 1 260.8 cm^{-1}, which is the second line of the Raman doublet for $J=67$, as discussed in (a) of Sec. III A 1. This probably gives a contribution to feature 5, but since the detuning between $\omega_{n'a}$ and ω_a is large (10 cm^{-1}), this contribution is small.

Two strong resonances are also contributed by the $v''=1$, $J=62|a\rangle$ level. These are $[Q(7-1), P(13-1), p(27-1)]62$ at 1 251.15 cm^{-1} and coinciding with feature 3, and $[q(7-1), P(13-1), P(27-1)]62$ coinciding with feature 4. Furthermore, an appreciable fraction of feature 3 may come from $[Q(7-1), p(13-1), P(27-1)]63$, which is a resonance of the (c) type in Sec. III A 1.

Downshifting ω_L by 0.3 cm^{-1} does not displace the vibrational resonances in the spectrum, but translates all the double electronic ones to the right by 0.3 cm^{-1}. Feature 1 therefore tends to merge with 2, forming line 6. The resulting enhancement offsets the loss due to ω_L moving away from ω_{na}, and the resonance remains very strong. The two contributions from $J=62$ are reduced appreciably as they move apart and also as a result of $\omega_{na} - \omega_L$ increasing, causing line 4 to disappear. Meanwhile, the $[Q,p,P]63$ resonance is little affected. It undergoes a slight splitting, thus contributing both to line 6 and to its weak shoulder 7.

Examination of the absorption spectrum about ω_L suggests possible contributions from $v''=2$, $J=112$, 113, 54, 55, 59, and 60. Similarly for $v''=0$, $J=117$, 118, 123 and $v''=1$, $J=114$, 119. Most of the corresponding CARS lines either appear out of the spectral region scanned, or present large laser, vibrational or anti-Stokes detunings, or have small Franck-Condon factors for their $\omega_{n'a}$ transitions. Nevertheless, many of these lines, although weak, give contributions between 1 249 and 1 252 cm^{-1}, and 1 258 and 1 261 cm^{-1}, which may explain most of the weaker features that have been left unaccounted for.

The above discussion can only be semiquantitative at present. A precise analysis would require a computer simulation, taking into account the complex character of the various resonances (which requires the full evaluation of the complex transition moments to be carried out), thereby accurately representing the interference between the lines, and the resulting spectral distortions.

The measurements were conducted with laser powers not exceeding 10 kW, but still sufficient to cause saturation and Stark broadening. However, we have no evidence that these effects were present to any great extent. The sharper features have a linewidth on the order of 0.6 cm^{-1}, which is what we expect on the basis of Γ_{ba}, $\Gamma_{n'a}$ and laser bandwidth. Fluctuations due to the absence of a reference also probably account for a small fraction of the broadening. Because of transverse beam nonuniformity, and because the signal is integrated over a volume large compared to the focal zone, we expect both Stark broadening and population perturbations to be difficult to observe.[78,79] These phenomena will be investigated in the near future. It will also be necessary to adjust ω_L about the absorption lines with greater precision than now for an unambiguous interpretation of the spectra. Of great interest too will be the verification of the predictions on resonant CARS spectra excited in the continuum.

VI. CONCLUSION

In the present paper, we have considered in detail the utilization of electronic resonance in order to provide an enhancement of the CARS nonlinear susceptibility, with an important application in mind: improved detection sensitivity of CARS experiments in analytical chemistry. In the course of this investigation, we have uncovered some remarkable properties of resonant CARS which will have important applications in resonant Raman scattering studies and one-photon spectroscopy.

We have provided a discussion of the susceptibility based upon the density matrix and have introduced density-matrix perturbation diagrams to clearly interpret and classify the terms which arise in the susceptibility. Such diagrams uniquely specify the quantum processes involved in the development of the nonlinear polarization at ω_a. We have shown that two types of diagrams, which we have called parametric and nonparametric, contribute to the CARS susceptibility, and that the nonparametric ones occur in groups of three corresponding to three time-ordered possibilities of the interactions. Of these three possibilities, one is dominant due to the presence of a vibrational resonance; the other two, although small, can produce a shift of the electronic resonances pertaining to state $|b\rangle$.

In gases, resonant CARS spectroscopy is best performed by holding the laser frequency ω_L fixed on one of the absorption lines and tuning ω_S across the vibrational resonances. Two types of electronically enhanced Raman resonances are then observed: one is associated with the molecular levels responsible for the resonant absorption of ω_L, and one is associated with levels giving simultaneous vibrational and anti-Stokes resonances. In addition, double electronic resonances are also found.

The line shapes in resonant CARS have been analyzed by representing the susceptibility as a vector in the complex plane. We found, as in off-resonance CARS, that the extremity of this vector describes a circle when ω_L is held fixed and ω_S varied. The circle position and diameter depend on the amplitudes and relative phases of the one-photon resonant terms in the susceptibility. The circle model gives a simple visualization of the roles played by χ_{NR}, mixing ratio, detuning from resonance, and transition moments, in determining the spectral contour. Thus we were able to give simple interpretations of the results observed recently in liquids by using this model without resorting to numerical calculations. Resonant CARS spectra can be used to determine the relative magnitudes and phases of the cross products of transition moments between vibronic levels in the ground and the excited electronic state. This information can be retrieved from the contour of a given isolated line. The analysis of several lines in a resonant CARS spectrum will provide several products of transition moments and therefore allow one to determine the complex transition moments relative to one another. Equivalent experiments were recently proposed based on RRS.[80]

The excitation into dissociative continua was predicted to yield spectra resembling off-resonance spectra, without the double electronic resonances, and with enhancements comparable to or less than those obtained with discrete absorption lines. For these reasons, and because the spectral intensities do not depend upon the widths of the absorption lines, this type of excitation may prove more practical for the study of rapidly fluctuating media.

We have also discussed the dependence of line intensities upon rotational transition moments and collision broadening, and found the behavior to be appreciably different from the off-resonance behavior. The perturbation of populations by one-photon absorption and stimulated Raman scattering were considered in detail and the magnitude of the broadening of CARS features by the optical Stark effect was briefly studied. The experimental limitations, especially those concerning the maximum pump power densities, were listed. It appears that 100 MW/cm^2 constitutes a maximum in gases at STP.

By means of the diagrammatic analysis, the transient CARS regime resulting from the turning on and off the two pump fields are also easily depicted. The transient behavior of the most important contribution to the nonlinear polarization at ω_a has been discussed and compared with that of the polarization at ω_S which is related to resonant Raman scattering.

Finally, resonance-enhanced CARS in iodine molecules has been observed. The I_2 was at a partial pressure of 1 mb in air near STP. The pump at ω_L was below the dissociation continuum, close to the NaD line, and in a region where the absorption lines have all been identified. Several CARS resonances in the fifth overtone band were recorded and assigned. They correspond to the categories of double resonances predicted by the theory. One feature was almost a triple resonance. The enhancement in susceptibility was, for some of these lines, on the order of 400 as compared with simple diatomics excited off resonance.

The approach and conclusions of this paper could be transposed readily to related third-order effects like RIKE (1-3) and SGRS (4). Some of the aspects of SRGS have actually been discussed in the course of our presentation.

ACKNOWLEDGMENT

This research was supported in part by DRET (Contract No. 77/243). One of us (T.K.G.) gratefully acknowledges partial support from ARO Grant No. 75-C-0095.

APPENDIX A

Any time-ordered contribution to the density operator can be precisely defined and readily

written down by means of the associated diagram. We list here the rules permitting one to draw the diagrams and to calculate the associated terms for the impact and isolated line approximations in accordance with Refs. 21 and 22. Any time-ordered contribution to the nth order of perturbation of the density operator is associated with a diagram according to the following rules: (i) The time axis is drawn vertically. (ii) The time evolution of the wave function (*ket*) is plotted vertically to the left of this axis and that of the complex conjugate (*bra*) on the right, so that one can follow the time evolution of the density operator contribution along the time axis. (iii) The field interactions are represented in the standard way by vertices that are specified, respectively, as the photon creation or annihilation operators. Note here that each vertex is drawn at 45° to the tangent to the circle, and not to the time axis as was done in Refs. 21 and 22. (iv) The number of interactions (or vertices) on the *ket* side and on the *bra* side are specified, their total number being equal to the order of the perturbation n. (v) The time ordering of the interactions on the *ket* is specified relative to the interactions on the *bra*.

We consider the diagram of Fig. 3(a) to illustrate the utilization of the rules permitting one to calculate the associated steady state contribution to $P_{NL}^{(3)}(\omega_a, t)$. There are three relevant field interactions on this diagram, one of them on the *ket* side and the other two on the *bra* side. The first interaction occurs at time t_1 and is specified as a Stokes photon annihilation operator operating on the *bra* $\langle b|$. The second one occurs at time t_2 and is specified as a laser photon annihilation operator operating on the *ket* $|b\rangle$. The last one at time t_3 is specified as a laser photon creation operator operating on the *bra* $\langle n|$. Beginning at t_0 and tracing up the diagram, one introduces factors as follows: (i) The initial density matrix element $\rho_{bb}^{(0)}$. (ii) The transition moment associated with the first perturbation which results in a change of the molecular complex conjugate wave function from $\langle b|$ to $\langle n|: \langle b| - \vec{P} \cdot \hat{e}|n\rangle E_S^* e^{i\omega_S t} e^{-ik_S z}$. (iii) The propagation factor resulting from the simultaneous evolution of *bra* $\langle n|$ and *ket* $|b\rangle$ between t_1 and t_2: $1/\hbar(-\omega_{bn} + i\Gamma_{bn} - \omega_S)$. (iv) The transition moment associated with the second perturbation resulting in a change of the molecular wave function from $|b\rangle$ to $|n'\rangle: \langle n'| - \vec{P} \cdot \hat{e}|b\rangle E_L e^{-i\omega_L t} e^{+ik_L z}$. (v) The propagation factor resulting from the simultaneous evolution of *ket* $|n'\rangle$ and *bra* $\langle n|$ between t_2 and t_3: $1/\hbar(-\omega_{n'n} + i\Gamma_{n'n} + \omega_L - \omega_S)$. (vi) The transition moment associated with the last perturbation which brings the molecular state from $\langle n|$ to $\langle a|: \langle n| - \vec{P} \cdot \hat{e}|a\rangle E_L e^{-i\omega_L t + ik_L z}$. (vii) The propagation factor resulting from the evolutions of *bra* $\langle a|$ and *ket* $|n'\rangle$ between t_3 and t: $1/\hbar(-\omega_{n'a} + i\Gamma_{n'a} + \omega_a)$. (iii) If the number of field interactions on the *bra* side is even (odd) one must put a + (−) sign in front of the contribution of interest [that is a + sign in the case of Fig. 3(a)]. (ix) This gives the matrix element $\rho_{n'a}^{(3)}$ depicted in the diagram at time t. In order to obtain the associated contribution to $P_{NL}^{(3)}(\omega_a, t)$ as given by Eq. (4), one finally has to multiply by $\langle n'| \vec{P} \cdot \hat{e}|a\rangle$. The fourth vertex in the diagram is of no use in calculating $P_{NL}^{(3)}(\omega_a, t)$. It represents the coupling between the field at ω_a and $P_{NL}^{(3)}(\omega_a, t)$, which results in either absorption or emission at ω_a, depending upon the respective phases of all the fields including E_a (see Sec. II B 2).

Inclusion of damping in the diagrams implies an averaging of the corresponding terms over all the statistical parameters. In the impact and isolated line approximation[21,22,30,32] and with the assumption of Lorentzian broadening, the diagrammatic representation of damping is equivalent to the damping approximation (3) used in the density matrix calculation.

APPENDIX B

The rate of change of the vibrational population resulting from four-wave mixing (such as CARS) or stimulated Raman scattering can be expressed quite generally in terms of the fourth order perturbation diagonal density matrix terms $\rho_{aa}^{(4)}(\omega, t)$ and $\rho_{bb}^{(4)}(\omega, t)$. We write it as:

$$\frac{\partial}{\partial t}\Delta(\omega, t) = \frac{\partial}{\partial t}\rho_{aa}^{(4)}(\omega, t) - \frac{\partial}{\partial t}\rho_{bb}^{(4)}(\omega, t). \tag{B1}$$

In order to calculate these terms, all fields including $E_a(z,t)$ must be written down explicitly. In general $E_a(z,t)$ is arbitrary; however, assuming the medium to be homogeneous, neglecting homogeneous solutions of the wave equation, and assuming it to be zero at the input boundary, $E_a(z,t)$ can be given a simple expression as a function of $E_L(z,t)$, $E_S(z,t)$, and $\chi^{(3)}(\omega_a)$:

$$E_a(z,t) = \frac{2i\pi\omega_a}{c}\chi^{(3)}(\omega_a)E_L^2(z,t)E_S^*(z,t)z. \tag{B2}$$

This particular expression is the basis of the interpretation of the energy level diagrams of Fig. 4. Equation (B1) can be calculated either by iterative integrations of Eq. (2) or from the time-ordered diagrams depicting the nonlinear polarizations at ω_a (Figs. 1–3), ω_L and ω_S. We consider here the stationary nonoscillating zero-frequency components $\rho_{aa}^{(4)}(0,t)$ and $\rho_{bb}^{(4)}(0,t)$ as they give the major contribution. One has for $\rho_{aa}^{(4)}(0,t)$:

$$\frac{\partial}{\partial t}\rho_{aa}^{(4)}(0,t)=\frac{-2}{\hbar}\mathrm{Im}\sum_n \mu_{an}[\rho_{na}^{(3)}(\omega_a,t)E_a^*\exp i(\omega_a t-k_a z)+\rho_{na}^{(3)}(\omega_L,t)E_L^*\exp i(\omega_L t-k_L z)$$
$$+\rho_{na}^{(3)}(\omega_S,t)E_S^*\exp i(\omega_S t-k_S z)]-\Gamma_{aa}\rho_{aa}^{(4)}(0,t). \tag{B3}$$

The three terms on the right hand side of (B3) are, respectively, associated with $P_{NL}^{(3)}(\omega_a,t)$, $P_{NL}^{(3)}(\omega_L,t)$, and $P_{NL}^{(3)}(\omega_S,t)$; both parametric and nonparametric time-ordered diagrams contribute to each of these terms. Each term $\rho_{na}^{(3)}(\omega,t)$ arises from two distinct second order contributions, i.e., nondiagonal term $\rho_{ba}^{(2)}$ at frequency $\omega_L-\omega_S$ and diagonal terms $\rho_{nn}^{(2)}$, $\rho_{aa}^{(2)}$, $\rho_{bb}^{(2)}$ at frequencies $0, 2\omega_L$, and $\omega_L-\omega_S$. The diagonal terms become important only near electronic resonances. An analogous expression can be obtained for $(\partial/\partial t)\rho_{bb}^{(4)}(0,t)$.

As an example, we give the expression for the $\rho_{ba}^{(2)}$ contribution to the population changes due to resonant CARS, discarding the terms possessing one or more antiresonances

$$\frac{\partial}{\partial t}\Delta(0,t)+\Gamma_{aa}\rho_{aa}^{(4)}(0,t)-\Gamma_{bb}\rho_{bb}^{(4)}(0,t)=\frac{1}{\hbar^4}\Bigg\{-2\,\mathrm{Im}\frac{E_L^2E_S^*E_a^*\exp i\delta kz}{\omega_{ba}-\omega_L+\omega_S-i\Gamma_{ba}}$$
$$\times\sum_{n'}\frac{\mu_{an'}\mu_{n'b}}{\omega_{n'a}-\omega_a-i\Gamma_{n'a}}$$
$$\times\sum_n\left[(\rho_{aa}^{(0)}-\rho_{nn}^{(0)})\frac{\mu_{bn}\mu_{na}}{\omega_{na}-\omega_L-i\Gamma_{na}}-(\rho_{bb}^{(0)}-\rho_{nn}^{(0)})\frac{\mu_{bn}\mu_{na}}{\omega_{nb}-\omega_S+i\Gamma_{nb}}\right]$$
$$+2\,\mathrm{Im}\frac{E_L^2E_S^*E_a^*\exp i\delta kz}{\omega_{ba}-\omega_L+\omega_S+i\Gamma_{ba}}\sum_{n'}\frac{\mu_{bn'}\mu_{n'a}}{\omega_{n'a}-\omega_L+i\Gamma_{n'a}}$$
$$\times\sum_n\left[(\rho_{aa}^{(0)}-\rho_{nn}^{(0)})\frac{\mu_{an}\mu_{nb}}{\omega_{na}-\omega_a+i\Gamma_{na}}\right.$$
$$\left.-(\rho_{bb}^{(0)}-\rho_{nn}^{(0)})\frac{\mu_{an}\mu_{nb}}{\omega_{nb}-\omega_L-i\Gamma_{nb}}\right]$$
$$+2\,\mathrm{Im}\frac{E_L^2E_S^*E_a^*\exp i\delta kz}{\omega_{ba}-\omega_L+\omega_S+i\Gamma_{ba}}$$
$$\times\sum_{n'}\frac{\mu_{bn'}\mu_{n'a}}{\omega_{n'b}-\omega_S-i\Gamma_{n'b}}$$
$$\times\sum_n\left[(\rho_{aa}^{(0)}-\rho_{nn}^{(0)})\frac{\mu_{an}\mu_{nb}}{\omega_{na}-\omega_a+i\Gamma_{na}}-(\rho_{bb}^{(0)}-\rho_{nn}^{(0)})\frac{\mu_{an}\mu_{nb}}{\omega_{nb}-\omega_L-i\Gamma_{nb}}\right]$$
$$-2\,\mathrm{Im}\frac{E_L^2E_S^*E_a^*\exp i\delta kz}{\omega_{ba}-\omega_L+\omega_S-i\Gamma_{ba}}$$
$$\times\sum_{n'}\frac{\mu_{an'}\mu_{n'b}}{\omega_{n'b}-\omega_L+i\Gamma_{n'b}}\sum_n\left[(\rho_{aa}^{(0)}-\rho_{nn}^{(0)})\frac{\mu_{bn}\mu_{na}}{\omega_{na}-\omega_L-i\Gamma_{na}}\right.$$
$$\left.-(\rho_{bb}^{(0)}-\rho_{nn}^{(0)})\frac{\mu_{bn}\mu_{na}}{\omega_{nb}-\omega_S+i\Gamma_{nb}}\right]\Bigg\}, \tag{B4}$$

where δk is the phase mismatch, *ie* $\delta k=2k_L-k_S-k_a$. There are four main terms in (B4), the first two being $(\partial/\partial t)\rho_{aa}^{(4)}(0,x)$ and the others $(\partial/\partial t)\rho_{bb}^{(4)}(0,t)$. In the former, the contributions proportional to $\rho_{aa}^{(0)}$ can be visualized and calculated with a parametric time-ordered diagram, while those proportional to $\rho_{bb}^{(0)}$ correspond to the nonparametric time-ordered diagrams; it is the opposite for the last two terms.

Far below electronic resonances, the population change $(\partial/\partial t)\Delta(0,t)$ resulting from CARS corresponds to the two vibrational quanta exchanged between the radiation fields and the molecules in the nonparametric process of Fig. 4(b). In that case, the one-photon resonance denominators in (B4) are nearly equal and factor out, so that the vibrational perturbation can be expressed in terms of the CARS susceptibility

$$\frac{\partial}{\partial t}\Delta(0,t)=\frac{-4}{\hbar^4}\mathrm{Im}\left\{E_L^2E_S^*E_a^*\,e^{i\delta kz}\left[\frac{\rho_{aa}^{(0)}-\rho_{bb}^{(0)}}{\omega_{ba}-\omega_L+\omega_S-i\Gamma_{ba}}\sum_{n'}\left(\frac{\mu_{an'}\mu_{n'b}}{\omega_{n'a}-\omega_a}+\frac{\mu_{an'}\mu_{n'b}}{\omega_{n'b}+\omega_a}\right)\right.\right.$$
$$\left.\left.\times\sum_{n}\left(\frac{\mu_{bn}\mu_{na}}{\omega_{na}-\omega_L}+\frac{\mu_{bn}\mu_{na}}{\omega_{na}+\omega_S}\right)-\mathrm{c.c}\right]\right\}$$
$$\propto \mathrm{Im}\chi_R(E_L^2E_S^*E_a^*\,e^{i\delta kz}+\mathrm{c.c.})\,. \tag{B5}$$

Combining (B2) and (B5) one gets[19,36] $(\partial/\partial t)\Delta(0,t)\propto|\mathrm{Im}\chi_R|^2N_L(N_SN_a)^{1/2}$, where N_L, N_S, and N_a are the photon fluxes per unit area per unit time at ω_L, ω_S, and ω_a, respectively. In that case the rate of population change associated with CARS and depicted in Fig. 4(b) appears as proportional to $|\mathrm{Im}\chi_R|^2$.

*Permanent Address: Department of Electrical Engineering and Computer Sciences and the Electronics Research Laboratory, University of California, Berkeley Calif. 94720 (U. S. A.).

[1]D. Heiman, R. Hellwarth, M. Levenson, and G. Martin, Phys. Rev. Lett. 36, 189 (1976).
[2]M. D. Levenson and J. J. Song, J. Opt. Soc. Am. 66, 641 (1976).
[3]G. L. Eesley, M. D. Levenson, and W. M. Tolles, IEEE J. Quant. Elec. QE-14, 45 (1978).
[4]A. Owyoung and E. D. Jones, Opt. Lett. 1, 152 (1977).
[5]P. Régnier and J.-P. Taran, Appl. Phys. Lett. 23, 240 (1973).
[6]M. Péalat, S. Druet, B. Attal, and J.-P. Taran, *Temperature and Concentration Measurements in Reactive Media by CARS* (MIT, Cambridge, Mass., 1976).
[7]W. B. Roh, P. W. Schreiber, and J.-P. Taran, Appl. Phys. Lett. 29, 174 (1976).
[8]J. W. Nibler, J. R. McDonald, and A. B. Harvey, *Proceedings of the Fifth International Conference on Raman Spectroscopy*, edited by E. D. Schmidt (Schulz, Freiburg in Breisgau, 1976), p. 717.
[9]J. W. Nibler, J. R. McDonald, and A. B. Harvey, Opt. Commun. 18, 371 (1976); W. M. Shaub, J. W. Nibler, and A. B. Harvey, J. Chem. Phys. 67, 1883 (1977).
[10]S. A. Akhmanov, A. F. Bunkin, S. G. Ivanov, N. I. Koroteev, A. I. Kovrigin, and I. K. Shumay, in *Tunable lasers and Applications*, edited by A. Mooradian, T. Jaeger, and P. Stokseth (Springer-Verlag, Berlin 1976), p. 389.
[11]J. J. Barrett and R. F. Begley, Appl. Phys. Lett. 27, 129 (1975).
[12]M. A. Henessian, L. Kulevskii, and R. L. Byer, J. of Chem. Phys. 65, 5530 (1976).
[13]V. I. Fabelinsky, B. B. Krynetsky, L. A. Kulevsky, V. A. Miskin, A. M. Prokhorov, A. D. Savel'Ev, and V. V. Smirnov, Opt. Commun. 20, 389 (1977); B. B. Krynetsky, L. A. Kulevsky, V. A. Miskin, A. M. Prokhorov, A. D. Savel'Ev, and V. V. Smirnov, *ibid.* 21, 225 (1977).
[14]A. Hirth and K. Volrath, Opt. Commun. 18, 213 (1976).
[15]I. Chabay, G. K. Klauminzer, and B. S. Hudson, Appl. Phys. Lett. 28, 27 (1976).
[16]J. Nestor, T. G. Spiro, and G. Klauminzer, Proc. Nat. Acad. Sci. U. S. A. 73, 3329 (1976); B. Hudson, W. Hetherington III, S. Cramer, I. Chabay, and G. Klauminzer, *ibid.* 73, 3798 (1976).
[17]A. Laubereau, G. Wochner, and W. Kaiser, Opt. Commun. 17, 91 (1976); Phys. Rev. A 13, 2212 (1976); A. Penzkofer and W. Kaiser, Opt. Quant. Elect. 9, 315 (1977).
[18]F. Moya, S. Druet, M. Péalat, and J.-P. Taran, in Experimental Diagnostics in Gas Phase Combustion Systems, Progress in Astronaut. and Aeronaut. 53, edited by B. T. Zinn (American Institute of Aeronautics and Astronautics, Princeton, New Jersey, 1977), p. 549.
[19]J.-P. Taran, in *Tunable Lasers and Applications*, edited by A. Mooradian, T. Jaeger, and P. Stokseth, (Springer-Verlag, Berlin, 1976), p. 378.
[20]M. D. Levenson and N. Bloembergen, Phys. Rev. B 10, 4447 (1974); R. T. Lynch Jr., S. D. Kramer, H. Lotem, and N. Bloembergen, Opt. Commun. 16, 372 (1976).
[21]S. Y. Yee and T. K. Gustafson, Phys. Rev. A (to be published).
[22]S. Y. Yee, T. K. Gustafson, S. Druet, and J.-P. Taran, Opt. Commun. 23, 1 (1977).
[23]Y. R. Shen, Phys. Rev. B 9, 622 (1974); Y. R. Shen *ibid.* 14, 1772 (1976).
[24]N. Bloembergen, *Nonlinear Optics* (Benjamin, New York, 1965).
[25]P. N. Butcher, in *Nonlinear Optical Phenomena* (Ohio State University Engineering, Columbus, (1965).
[26]R. W. De Witt, A. B. Harvey, and W. M. Tolles, Theoretical Development of Third-Order Susceptibility as Related to Coherent Anti-Stokes Raman Spectroscopy, NRL Memorandum Report 3260 (1976) (unpublished).
[27]S. Druet, Diffusion Raman Anti-Stokes Cohérente au voisinage des résonances électroniques, thesis Orsay, 1976. Available as ONERA Technical Note No. 1976-6, and, in English, as European Space Agency Technical Translation No. ESA TT 371 (1977) (unpublished).
[28]J. Hertz, A. Lau, M. Pfeiffer, and W. Werncke, in Lasers in Chemistry, Conference Digest, London, 1977 (unpublished), p. 399; A. Lau, M. Pfeiffer, and W. Werncke, Opt. Commun. 23, 59 (1977).
[29]H. Lotem, R. T. Lynch, Jr., and N. Bloembergen, Phys. Rev. A 14, 1748 (1976).
[30]M. Baranger, Phys. Rev. 111, 494 (1958).
[31]J. Fiutak and J. Van Kranendonk, C. J. Phys. 40, 1085 (1962).
[32]A. Omont, E. W. Smith, and J. Cooper, Astrophys. J.

175, 185 (1972).
[33]C. J. Bordé, C. R. Acad. Sc. Paris, t. 282, Series B, 341 (1976); C. J. Bordé in *Laser Spectroscopy III, Proceedings of the Third International Conference*, edited by J. L. Hall and J. L. Carlsten (Springer-Verlag, New York, 1977), p. 121.
[34]R. P. Feynman, *Quantum Electrodynamics* (Benjamin, New York, 1962), p. 19–22.
[35]R. T. Lynch, Jr., H. Lotem, and N. Bloembergen, in "Lasers in Chemistry" Conference Digest, London, 1977, p. 1 (unpublished); N. Bloembergen, H. Lotem, and R. T. Lynch, Jr., "Lineshapes in Coherent Resonant Raman Scattering"in *Raman 50th Jubilee Volume of the Indian Journal of Pure and Applied Physics* (to be published). R. T. Lynch, Jr., thesis (Harvard University, 1977) (unpublished)
[36]F. Moya, Application de la Diffusion Raman Anti-Stokes Cohérente aux mesures de concentrations gazeuses dans les écoulements, thesis, Orsay, available as ONERA Technical Note No. 1975-13, and in English, as European Space Agency Technical Translation No. ESA TT 331 (1976) (unpublished).
[37]This was not correctly asserted in Druet's thesis (Ref. 27), where Fig. 12 does not make sense.
[38]In the case of Raman Scattering, one observes a similar decoupling and Fermi's Golden Rule then applies.
[39]If one takes Lorentzian distributions for the g's and makes the damping approximation (11), then one finds the non-time-ordered result obtained in Sec. II B.
[40]M. Jacon, in *Advances in Raman Spectroscopy* (Heyden and Son, London, 1973), Vol. 1, p. 325.
[41]M. Berjot, M. Jacon, and L. Bernard, Opt. Commun. 4, 246 (1971).
[42]D. L. Rousseau and P. F. Williams, J. Chem. Phys. 64, 3519 (1976).
[43]J. W. Nibler, W. M. Shaub, J. R. McDonald, and A. B. Harvey, *Vibrational Spectra and Structure*, 6, edited by J. R. Durig (Elsevier, New York, 1977).
[44]M. A. Yuratich and D. C. Hanna, Mol. Phys. 33, 671 (1977).
[45]L. A. Carreira, L. P. Goss, and T. B. Malloy Jr., J. Chem. Phys. 66, 4360 (1977).
[46]R. T. Lynch, Jr., H. Lotem, and N. Bloembergen, J. Chem. Phys. 66, 4250 (1977).
[47]F. Moya, S. Druet, and J.-P. Taran, Opt. Commun. 13, 169 (1975).
[48]S. Barak and S. Yatsiv, Phys. Rev. A 3, 382 (1971).
[49]R. L. Brown and W. Klemperer, J. Chem. Phys. 41, 3072 (1964).
[50]A. Chutjian and T. C. James, J. Chem. Phys. 51, 1242 (1969).
[51]B. R. Mollow, Phys. Rev. A 5, 1522 (1972); 15, 1023 (1977).
[52]C. Cohen Tannoudji and S. Reynaud, J. Phys. B 10, 365 (1977).
[53]J. L. Carlsten, A. Szöke, and M. G. Raymer, Phys. Rev. A 15, 1029 (1977).
[54]F. Schuda, C. R. Stroud Jr., and M. Hercher, J. Phys. B 7, L198 (1974).
[55]R. E. Grove, F. Y. Wu, and S. Ezekiel, Phys. Rev. A 15, 227 (1977).
[56]N. Skribanowitz, M. J. Kelly, and M. S. Feld, Phys. Rev. A 6, 2302 (1972).
[57]S. Feneuille and M. G. Schweighofter, J. Phys. 36, 781 (1975).
[58]J. L. Picqué and J. Pinard, J. Phys. B 9, L77 (1976).
[59]J. E. Bjorkholm and P. F. Liao, Opt. Commun. 21, 132 (1977).
[60]C. M. Penney, L. M. Goldman, and M. Lapp, Nat. Phys. Sci., 235, 110 (1972); H. Rosen, P. Robrish, and O. Chamberlain, Appl. Opt. 14, 2703 (1975).
[61]W. Holzer, W. F. Murphy, and H. J. Bernstein, J. Chem. Phys. 52, 339 (1970); 52, 499 (1970); M. Ber-Berjoth, thesis (Université de Reims) (unpublished).
[62]D. G. Fouche and R. K. Chang, Phys. Rev. Lett. 29, 536 (1972); R. L. St Peters, S. D. Silverstein, M. Lapp, and C. M. Penney, *ibid.* 30, 191 (1973); D. G. Fouche, A. Herzenberg, and R. K. Chang, J. Appl. Phys. 43, 3846 (1972).
[63]S. D. Silverstein and R. L. St Peters, Phys. Rev. A 9, 2720 (1974); M. Jacon and D. Van Labeke, Mol. Phys. 29, 1241 (1975).
[64]J. R. Solin and S. Merkelo, Phys. Rev. B 12, 624 (1975); 14, 1775 (1976).
[65]P. Robrish, H. Rosen, and O. Chamberlain, Phys. Lett. A 51, 434 (1975).
[66]Y. R. Shen, Rev. Mod. Phys. 48, 1–31 (1976).
[67]*Laser Spectroscopy III, Proceedings of the Third International Conference*, edited by J. L. Hall and J. L. Carlsten (Springer-Verlag, New York, 1977).
[68]M. Berjot and L. Bernard, in *Advances in Raman Spectroscopy* (Heyden and Son, London, 1973), Vol. 1, p. 343.
[69]S. Mukamel and J. Jortner, J. Chem. Phys. 62, 3609 (1975); S. Mukamel, A. Ben Reuven, and J. Jortner, Phys. Rev. A 12, 947 (1975).
[70]A. Herzenberg and E. Stryjewski, Phys. Rev. A 15, 234 (1977).
[71]J. D. Simmons and J. T. Hougen, J. Res. Nat. Bur. Stand. A 81, 25 (1977).
[72]S. Gerstenkorn and P. Luc, Atlas de la Molécule d'Iode (unpublished).
[73]J.-P. Taran, in Ref. 67, p. 315.
[74]B. Attal, O. Schnepp, and J.-P. Taran, Opt. Commun. 24, 77 (1978).
[75]D. A. Shirley and W. F. Giauque, J. Am. Chem. Soc. 81, 4778 (1959).
[76]S. Gerstenkorn and P. Luc, "Atlas du Spectre d'Absorption de la Molécule d'Iode", Laboratoire Aimé Cotton CNRS II, 91405 Orsay, France (unpublished); line assignments of the spectrum about ω_L are also from the same authors (private communication).
[77]W. Keifer and H. J. Bernstein, J. Mol. Spectrosc. 43, 366 (1972).
[78]A. B. Rodrigo and R. M. Measures, IEEE J. Quant. Electron. QE9, 972 (1973).
[79]J. W. Daily (unpublished).
[80]C. L. Pan, C. Y. She, W. M. Fairbank, Jr., and K. W. Billman, IEEE J. Quant. Elec. QE13, 763 (1977).